The Stejskal–Tanner Equation Generalized for Any Gradient Shape—An Overview of Most Pulse Sequences Measuring Free Diffusion

DAVY SINNAEVE

Department of Organic Chemistry, Ghent University, Krijgslaan 281 S4, B-9000 Gent, Belgium

ABSTRACT: The widely known Stejskal–Tanner (ST) equation is central to any diffusion NMR or so-called pulsed gradient spin-echo experiment, describing the signal attenuation due to loss of coherence caused by diffusion as a function of the experimental parameters. What is less widely known is that the equation itself is not invariable when applying different pulse sequences or different gradient pulse shapes and should thus be modified accordingly. This concept is not new, but nevertheless experimentalists applying diffusion NMR in their research often overlook or are completely oblivious to this fact. In this article, the derivation of the ST equation through the Bloch–Torrey equations is discussed in detail, followed by a discussion of the most basic NMR experiments that measure free diffusion. This derivation is performed here in a novel way, leading to expressions for the ST equation that do not assume any gradient shape beforehand, leaving only a few parameters that are determined solely by the gradient pulse shape. This new approach to presenting the ST equation increases awareness of its dependence on gradient shape. Moreover, it relieves designers of future diffusion NMR pulse sequences of struggling with the cumbersome task of deriving and reporting the equation for each gradient shape separately. A quick reference table of the ST equation for the basic diffusion NMR pulse sequences for any gradient shape is given, as well as an overview for most other diffusion NMR pulse sequences described in the literature. © 2012 Wiley Periodicals, Inc. Concepts Magn Reson Part A 40A: 39–65, 2012.

INTRODUCTION

Since their introduction two decades ago, the widespread availability of high resolution NMR probes capable of applying moderate amplitude magnetic pulsed field gradients (PFGs) has facilitated the measurement of translational diffusion coefficients with NMR spectroscopy, leading to extensive methodological development and application. The ability to measure the diffusion coefficient in a relatively straightforward manner combined with all the other structural information that NMR can provide creates a large potential for the study of hydrodynamic properties and molecular interactions. The diffusion coefficient's dependence on size and shape can for example provide insight into the nature and molar mass of the supramolecular complexes formed (1–4), or indicate whether a protein is globular or unstructured (5). The measured diffusion coefficient is also sensitive to chemical exchange processes (6–8), providing a method to study this phenomenon in addition to methods based on chemical shift or relaxation, such as line shape analysis or relaxation dispersion. As for the chemical shift, slow, intermediate, and fast exchange regimes can be distinguished relative to a diffusion time-scale. In the case of chemical exchange between two or more states that is fast compared to the time over which diffusion is measured, an averaged value for the diffusion coefficient will be measured. When the diffusion coefficients of both states are sufficiently different (e.g., protein−ligand interactions), both a qualitative and quantitative assessment of the binding interaction can be obtained (9, 10). Typical examples are the determination of the critical micellar concentration (CMC) of surfactants (11) or the binding of small molecules with micelles or vesicles (12–14). In the situation of slow exchange on the diffusion time-scale, but where the resonances of the different states cannot be resolved within the 1D spectrum, the analysis of the resulting multiexponential signal decay can provide the populations of the different exchanging components (15, 16). Diffusion NMR has also been applied to the study of the kinetics of chemical reactions that occur slowly relative to the diffusion measurement (17, 18). Finally, in the case of intermediate exchange, the multiexponential decay will, besides the populations, provide information concerning the rate of the exchange process (19–21).

Diffusion NMR measurements have also found application in the analysis of mixtures. By correlating the chemical shift information to the molecular translational diffusion coefficient in a so-called 2D DOSY plot (diffusion ordered spectroscopy) (22), the signals in the NMR spectrum can in principle be resolved from one another according to the molecules they originate from, provided the difference in diffusion coefficient is sufficient. This method has found its way to the chemist's NMR toolbox for structure analysis. It allows the components of a mixture to be quickly identified and their individual NMR spectra to be separated. Some examples of applications of this so-called virtual separation technique can be found in combinatorial chemistry (1, 23), analysis of biological fluids (24), food science (25, 26), and polymer mixtures (24, 27), to name but a few.

The theoretical and methodological aspects of diffusion NMR have previously been covered in several reviews (24, 28–31) and a recent book by Price (32). Diffusion NMR experiments in their most common form involve the application of constant magnetic field gradients—i.e., a linearly varying magnetic field—along the longitudinal axis of the sample. The experiment provides a series of 1D NMR spectra in which the intensity of each signal experiences an attenuation E_{diff} according to the Stejskal–Tanner (ST) equation (33) on increasing the magnetic field gradient strength g. The most common form of this equation, assuming free diffusion, is a Gaussian decay function

$$E_{\text{diff}} = e^{-D\gamma_{\text{eff}}^2\delta^2\sigma^2 g^2\Delta'} \qquad [1]$$

in which D is the translational diffusion coefficient of the molecule to which the signal belongs, γ_{eff} is a linear combination of the gyromagnetic ratios of the nuclei studied depending on the coherence transfer pathway (CTP) of the experiment, δ is the PFG duration (i.e., the time during which the gradients were switched on) and σ is the gradient shape factor (*vide infra*). The diffusion delay Δ is the time during which the molecular diffusion can induce its effect, while Δ' is this same delay corrected by an amount that depends on the specific pulse sequence and gradient shape used (*vide infra*). To measure the translational diffusion coefficient, several 1D spectra are recorded at various gradient strengths g, resulting in an attenuation for each signal. Fitting Eq. [1] to these signal attenuations then provides the diffusion coefficients of the molecules associated with these signals. When signals arising from molecules with different diffusion coefficients overlap in the spectrum, the process to resolve the multiple diffusion coefficients becomes significantly more involved and over the years several processing techniques have been described to deal with this issue. For further introduction into this matter, the reader is directed to a recent overview provided by Nilsson (34) and the references therein.

From an experimental point of view, a whole arsenal of pulsed gradient spin echo (PGSE) or pulsed gradient stimulated echo (PGSTE) pulse sequences has been proposed to perform the diffusion NMR experiment, each with their own merits or special attribute and drawbacks. The choice of pulse sequence does have an impact on the ST equation however. In most cases this is limited to the Δ' value, but some pulse sequences can even induce a decay that does not follow the general dependence on g given in Eq. [1] (*vide infra*) (*35*). Moreover, for practical reasons, gradient pulses are often applied with a certain shape, further influencing Δ' and the shape factor σ in the equation. The intent of this article is to provide an overview of the most common and important classes of diffusion NMR pulse sequences and for each of them evaluate the exact form of the ST equation as a function of the given gradient shape. Indeed, examples can be found in literature, even at the level of diffusion NMR pulse sequence design (*36*, *37*), where authors seem to overlook the non-standard form of the ST equation required in their experimental set-up or state a version of the ST equation that is not in accordance to the applied gradient shape reported in the experimental section. Especially in the case when Δ does not differ by several orders of magnitude to δ, this will influence the extracted diffusion coefficient value, leading to erroneous results.

After briefly introducing the basic principles of how magnetic field gradients influence the magnetization and the purpose of introducing a shape to these gradient pulses, the impact of unrestricted molecular translational motion on any gradient experiment will be discussed, followed by the introduction to and solution of the Bloch–Torrey equations. Here, the ST equation will be derived in a generalized fashion for the most common pulse sequences in such a way that it does not assume the choice of gradient shape. This new way of presenting the ST equation has the advantage that when new diffusion pulse sequences are introduced, an appropriate ST equation fit to cover all gradient shapes can be introduced, avoiding the need to provide the resulting ST equation for every or only one selected gradient shape. Finally, a practical overview is provided for most pulse sequence and gradient shape combinations, offering a quick practical reference. Although the importance of taking the gradient shape into account has been pointed out multiple times in the past (*24*, *29*, *38*, *39*), the explicit results for many of the common pulse sequences have never been presented before, most likely due to the rigorous mathematical derivation that is associated. For this reason, many researchers who are not experts in the theoretical

background of diffusion NMR measurements, but do regularly apply these experiments in their research, might not always be aware of the correct equation for their choice of experimental set-up. In addition, researchers who are more specialized in this area will hopefully welcome this overview, as it will save them time by avoiding extensive mathematical derivations. Finally, it should be mentioned that those who are familiar with computer algebra software such as Maple or Mathematica can, as an alternative, quickly obtain the correct ST equation after going through some programming (*29*, *40*).
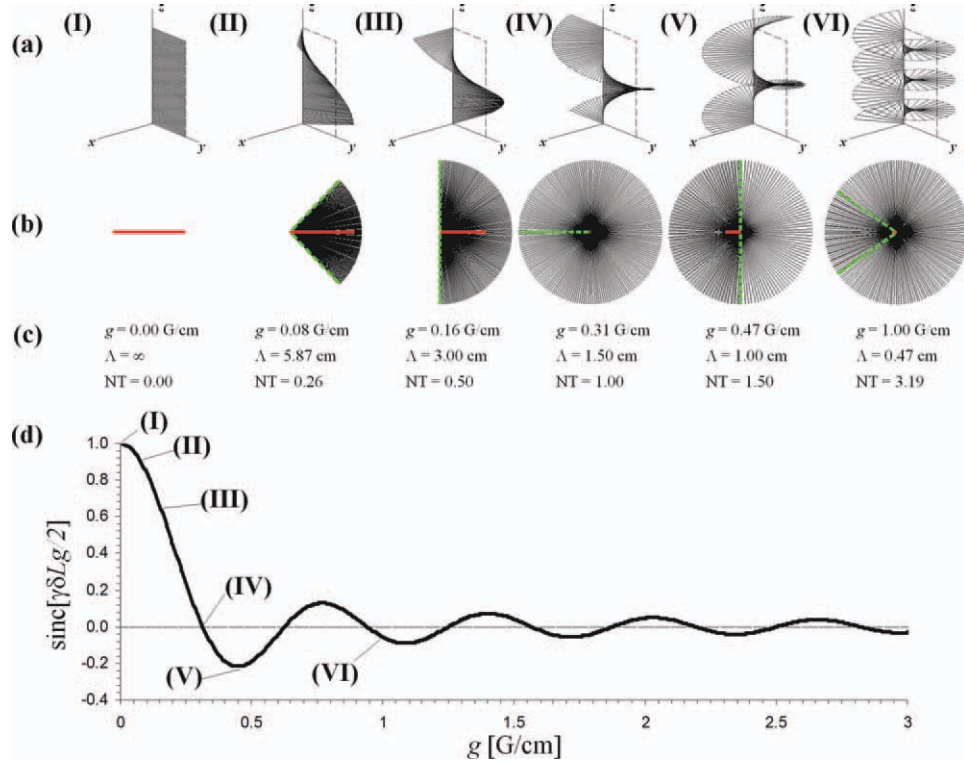
MAGNETIC FIELD GRADIENTS AND GRADIENT SHAPES

When describing the ideal NMR experiment, the static magnetic field B_0 is assumed to be homogeneous over the entire sample. When this is not the case, the spin coherence—i.e., the extent to which the different spins add up constructively to the total signal—will disappear much faster. This is because spins at different positions in the sample will no longer precess with the same angular velocity around the magnetic field and thus develop a phase difference relative to each other. Fortunately, a homogenous magnetic field can be achieved to a reasonable extent with modern NMR instruments. However, there are many NMR experiments (*41*) that benefit from temporarily destroying the homogeneity of the magnetic field in a controlled manner by applying a constant magnetic field gradient—i.e., a linearly varying magnetic field—created by a specially designed coil (*30*). In what follows, the effect on the detected signal of such a gradient will be discussed first.

Assume the presence of a constant magnetic field gradient along the z-axis of the sample with a strength g, i.e., the magnetic field varies with a slope g. The total precession angular frequency of the magnetization then becomes position dependent during this gradient, according to

$$\omega_{\text{tot}}(z) = -\gamma(B_0 + gz) = \omega_0 - \gamma gz.\qquad [2]$$

In all that follows, a rotating frame with angular frequency ω_0 is considered, so that only the gradient induced precession $-\gamma gz$ needs to be taken into account. When applying the gradient for a time δ, the total angle over which the magnetization will have precessed within the rotating frame will be $-\gamma gz\delta$. Assuming that the transverse magnetization has its initial orientation along the y-axis, it would have evolved as

Figure 1 Simulation of the effect of a constant magnetic field gradient on the magnetization. On-resonance, transverse magnetization is visualized along various positions of the z-axis, corresponding to a 15 mm sample length. The initial magnetization (*I*) is along the y-axis and subjected to various magnetic field gradient strengths g during a 500 μs period. As the gradient strength increases from (*II*) to (*VI*), the magnetization precesses over larger phase angles and a helical pattern forms, as illustrated in part (a). The dephasing of the magnetization is demonstrated by the top views (b). Here; the vector sum of all the magnetization vectors, and thus the total detectable magnetization, is represented by the thick red line, while the green dotted lines represent the phase angles along the edges of the sample. The gradient strength g, the helix pitch Λ, and number of turns NT are given in (c). The relative intensity of the detectable magnetization follows a sinc function, as illustrated in (d).

$$M_Y \rightarrow M_Y \cos(\gamma g z \delta) + M_X \sin(\gamma g z \delta). \qquad [3]$$

The X- and Y-components of the transverse magnetization will thus depend on the position along the z-axis of the sample. When the entire sample length along the z-axis is considered, the end result is a helical pattern as illustrated in Fig. 1. The pitch Λ of this helix (the displacement along z required for a full turn) and the number of turns NT over a given sample length L are given by:

$$\Lambda = \frac{2\pi}{\gamma g \delta} \qquad [4]$$

$$NT = \frac{L}{\Lambda} = \frac{\gamma g L \delta}{2\pi}. \qquad [5]$$

The total detectable magnetization can be found by integration of Eq. [3] over the sample length L:

$$M_Y \int_{-L/2}^{L/2} [\cos(\gamma g z \delta)]dz + M_X \int_{-L/2}^{L/2} [\sin(\gamma g z \delta)]dz$$

$$= M_Y \frac{L}{2} \operatorname{sinc}\left(\frac{\gamma g L \delta}{2}\right). \qquad [6]$$

The detectable magnetization will remain along the y-axis in the rotating frame, while its intensity experiences a dampened oscillation under the form of a sinc function with increasing gradient strength g (Fig. 1). The detected signal will change sign each time the number of helix turns NT reaches an integer. When the gradient strength is sufficiently strong, the

number of helix turns will have increased so much that the relative amount of the magnetization not forming a complete helix turn (i.e., at the ends of the helix) will be insufficient to give rise to a detectable signal.

If after a time delay δ the polarity of the gradient is reversed, i.e., its strength becomes $-g$, the magnetization at every position z in Eq. [3] will be refocused to its original orientation after a second delay δ

$$
\begin{aligned}
M_Y &\cos(\gamma gz\delta) + M_x \sin(\gamma gz\delta) \\
&\rightarrow [M_Y \cos(\gamma gz\delta) - M_X \sin(\gamma gz\delta)] \cos(\gamma gz\delta) \\
&+ [M_X \cos(\gamma gz\delta) + M_Y \sin(\gamma gz\delta)] \sin(\gamma gz\delta) = M_Y.
\end{aligned}
$$
[7]

The loss of coherence in the magnetization due to magnetic field gradients is thus reversible. It is in this sense that they are applied as a tool to select the desired magnetization (i.e., the CTP) while eliminating the unwanted magnetization (coherence). This is achieved by getting the latter dephased at the end of the pulse sequence, while the desired magnetization is either never dephased or is refocused by the gradients (41). To this end, magnetic field gradients are commonly applied as PFGs, where the gradient is switched on for only a short time. This would then correspond to a rectangular shape of the PFG. However, it is not possible to generate a gradient pulse that switches instantaneously from zero to a stable value g because the gradient coil has a non-zero inductance (39). The rise and fall times of the gradient pulses are therefore not infinitely small and the rectangular shape is only approximated. Gradient pulses are therefore often applied with a certain non-rectangular shape, offering a more gradual gradient strength increase at the beginning and decrease at the end. The total precession angular frequency of the magnetization during the PFG from Eq. [2] then needs to be modified to include the shape function $s(\varepsilon)$

$$
\omega_{\text{tot}}(z, \varepsilon) = \omega_0 - \gamma gs(\varepsilon)z. \tag{8}
$$

Here, ε represents the progression or the extent through the gradient pulse, with $\varepsilon = 0$ and $\varepsilon = 1$, respectively, representing the start and the end of the pulse. The advantage is thus that the assumed shape of the gradients will correspond better to the actual one. Shaped gradient pulses may also serve to reduce the effects of eddy currents. These are electrical currents in the conducting metals of the NMR equipment itself caused by the time-dependent magnetic field gradients through induction. These currents then

again create time-dependent magnetic fields within the sample, which can distort the spectrum if they are still present during the acquisition time. The slower rates of change in gradient strength using shaped pulses help in reducing the eddy currents (24, 38). It should be mentioned that another often employed method to strongly reduce the effects of eddy currents is pre-emphasis. In essence, this is the introduction of a multiexponential decay function in the input electrical current that, when properly calibrated, compensates for the time-dependent effects of eddy currents and other electrical phenomena on the output magnetic field gradient (42).

A disadvantage of non-rectangular shaped pulses is that they are always less efficient in dephasing the magnetization than rectangular pulses of the same maximum gradient strength and duration. The efficiency of the gradient shape is expressed by its shape factor σ, which is the integral of the shape function $s(\varepsilon)$ over the extent of the gradient pulse

$$
\sigma = \int_0^1 s(\varepsilon)d\varepsilon. \tag{9}
$$

The shape factor for a rectangular shape is 1, representing maximum efficiency. The shape factor of a half sine bell-shaped gradient pulse is $2/\pi$ (≈ 0.64), implying that the dephasing of the magnetization will be 0.64 times less pronounced compared to a rectangular gradient pulse.

Table 1 introduces some possible gradient shapes and provides their shape factors. Two other gradient shape parameters, λ and κ, are included in the table as well, which will be relevant for the derivation of the ST equation later on. These are defined as

$$
\lambda = \frac{1}{\sigma} \int_0^1 S(\varepsilon)d\varepsilon \tag{10}
$$

$$
\kappa = \frac{1}{\sigma^2} \int_0^1 S^2(\varepsilon)d\varepsilon \tag{11}
$$

with

$$
S(\varepsilon) = \int_0^\varepsilon s(\varepsilon)d\varepsilon. \tag{12}
$$

The expression for the parameter λ can be rewritten, applying the method of integration by parts

Table 1 Overview of Possible Gradient Shape Functions and Calculated Values of Shape Parameters

	Rectangle	Sine bell	Square sine bell	Trapezoid	Smoothed rectangle
$s(\varepsilon)$	1	$\sin(\pi\varepsilon)$	$\sin^2(\pi\varepsilon)$	$\begin{cases} 10\varepsilon & 0 \le \varepsilon < \frac{1}{10} \\ 1 & \frac{1}{10} \le \varepsilon \le \frac{9}{10} \\ 10(1-\varepsilon) & \frac{9}{10} < \varepsilon \le 1 \end{cases}$	$\begin{cases} \sin^2[5\pi\varepsilon] & 0 \le \varepsilon < \frac{1}{10} \\ 1 & \frac{1}{10} \le \varepsilon \le \frac{9}{10} \\ \cos^2\left[5\pi\varepsilon - \frac{9}{10}\right] & \frac{9}{10} < \varepsilon \le 1 \end{cases}$
σ	1	$\frac{2}{\pi}$	$\frac{1}{2}$	$\frac{9}{10}$	$\frac{9}{10}$
λ	$\frac{1}{2}$	$\frac{1}{2}$	$\frac{1}{2}$	$\frac{1}{2}$	$\frac{1}{2}$
κ	$\frac{1}{3}$	$\frac{3}{8}$	$\frac{1}{3} + \frac{5}{8\pi^2}$	$\frac{8,483}{24,300}$	$\frac{422}{1,215} + \frac{23}{1,080\pi^2}$

$$\lambda = \frac{1}{\sigma}\left[\varepsilon S(\varepsilon)\big|_{\varepsilon=0}^{\varepsilon=1} - \int_0^1 \varepsilon s(\varepsilon)d\varepsilon\right].$$

$$= \frac{1}{\sigma}[\sigma - \sigma\mu]$$

$$= 1 - \mu$$
[13]

Here, μ is the expectation value of the variable ε when considering $s(\varepsilon)/\sigma$ as a normalized probability function. Most gradient shapes in use and all those listed in Table 1 are perfectly symmetrical, implying $\mu = \frac{1}{2}$ and consequently λ itself will always be $\frac{1}{2}$ in these cases.

THE BLOCH–TORREY EQUATIONS

When Hahn reported in 1950 the first spin-echo NMR experiments (43), which he used to remove the effects of static magnetic field inhomogeneity in T_2 relaxation measurements, he noted that the signal decayed faster than anticipated and interpreted this as due to the translational diffusion of the molecules bearing the nuclear spins during the experiment. A spin echo refocuses magnetization under the condition that each spin precesses with the same angular frequency before and after the refocusing pulse. If the spins have randomly moved during the echo to other regions where the magnetic field is different due to its inhomogeneity, the refocusing will no longer be complete, resulting in a loss of signal [Fig. 2(a)]. The main mechanism by which spins move position during the spin-echo experiment is the translational motion of the molecules carrying the spins. Recently, it has been shown that for large molecular entities such as fibrils, rotational motion can also provide a significant contribution to the signal attenuation by effectively inducing a translational motion of the spin (44). This work will consider only translational molecular motion however.

Diffusion is the net transport of molecules facilitated through their thermal translational motion, known as Brownian motion. When the molecular concentration c is non-uniform, i.e., a concentration gradient exists, the flux of molecules caused by diffusion has empirically been established to be proportional to the concentration gradient. This is known as Fick's first law of diffusion (assuming for simplicity only one-dimensional diffusion along the z-axis) (45)

$$J_z(z) = -D\frac{\partial c(z)}{\partial z}.$$
[14]
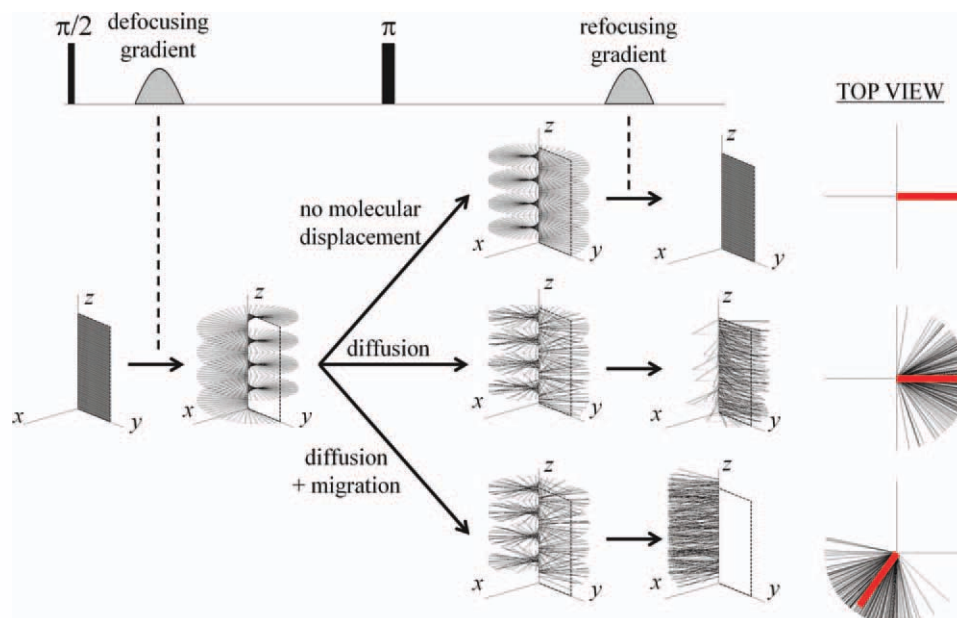
Figure 2 Simulation of the effects of diffusion and unidirectional translation on the magnetization during a PFG spin echo. The transverse magnetization, with initial position along the *y*-axis, is assumed here to be on-resonance. Here every line represents a single randomly selected spin at each position along the *z*-axis, as opposed to Fig. 1 where each line represents the magnetization, i.e., an ensemble of spins. The spins are dephased by a first, defocusing constant gradient pulse with 1.25 G/cm strength and 500 μs duration. The $180°_y$ pulse inverts the phase of the spins, so a second, refocusing gradient pulse with the same gradient strength, polarity, and duration will realign the spins to the *y*-axis, concluding the spin echo. The diffusion delay of the spin echo in this simulation was 10 s, chosen so long for the purpose of illustration. If during the spin-echo diffusion takes place (with a diffusion coefficient *D* of 4×10^{-9} m²/s), the molecules displace randomly across the *z*-axis, causing the helix pattern to disintegrate. When each line would have represented the magnetization instead of a single selected spin, the visual effect would be that the helix diameter attenuates due to diffusion, as is illustrated and explained in the Figure on page 80 in the book by Price (*32*). The refocusing of the second gradient pulse is now no longer ideal, leaving a stochastic, irreversible dephasing of the spins along the *z*-axis. The red line in the top view represents the vector sum of all spins. When additionally unidirectional translation takes place (here simulated with a velocity v_z of 8.7 cm/s, chosen so high for the purpose of illustration), the molecules and thus the helix pattern will experience a constant shift in position along the *z*-axis, causing a constant phase shift for all spins after the refocusing gradient. Note that since the magnetic field gradient is constant, the helix pitch is constant along the *z*-axis and therefore diffusion and unidirectional translation induce a *z*-position independent loss of coherence or phase shift, respectively.

The proportionality constant *D* is the translational diffusion coefficient, expressing the ease with which the molecules displace themselves through Brownian motion. It will be assumed here that it is both time- and position-independent. From Eq. [14], it is clear that the diffusion flux will work against the concentration gradient, thus creating a net transport from the highly concentrated to the less concentrated regions. This effectively makes the concentration distribution time-dependent until a uniform distribution is reached. The evolution over time of the concentration distribution is described by Fick's second law, which follows from Fick's first law combined with the principle of conservation of number of molecules (*45*)

$$\frac{\partial c(z,t)}{\partial t} = D \frac{\partial^2 c(z,t)}{\partial z^2}. \qquad [15]$$

Besides diffusion, other transport processes exist that can induce unidirectional translation. In contrast to Brownian motion, which is a stochastic thermal process, all molecules move in this case with an equal average local velocity caused by an external force. During a spin-echo experiment in an inhomogeneous

magnetic field, each spin will experience a different magnetic field before and after the refocusing pulse. However, provided that the translational velocity is constant within the volume element considered and the magnetic field inhomogeneity is linear, this difference will be equal for each spin within the volume element, leading to a perfect refocusing of all spins but with a net phase change [Fig. 2(b)]. Because the translational movement is unidirectional, the flux along the z-axis is proportional to the local concentration

$$J_z(z) = v_z c(z). \qquad [16]$$

The velocity of the translation along the z-axis v_z is here assumed to be both time- and position-independent. Applying a similar reasoning as for diffusion, the concentration distribution will change over time due to the translation as

$$\frac{\partial c(z,t)}{\partial t} = -v_z \frac{\partial c(z,t)}{\partial z}. \qquad [17]$$

One example of a translation process is electrophoretic migration of molecules carrying a net charge, where the external force is provided by an applied electrostatic field (46). Also the magnetic field gradients themselves may cause a small force to be exerted on the molecules via their nuclear magnetization. However, this force is usually too weak to induce any detectable motion and is therefore usually neglected (47). Another example is flow or convection of the whole bulk solution, for instance driven by pressure through a capillary. In an NMR tube, natural convection can also be induced by temperature gradients that induce unequal density over the sample. This can lead to convection cells, where part of the fluid moves upwards and the other part downwards. The profiles of these convective flows and the velocity distributions have been investigated by Jerschow (48) and Loening and Keeler (49). In the middle of this convection cell, where the active coil volume is located, the flows are laminar and more or less parallel to the z-axis. It can be assumed that in this region, the z-components of the velocity v_z of the flows are constant with both time and—at least locally—with z-position. Despite a distribution of velocities along the z-axis that exists within the xy-plane, Eq. [17] still holds for each particular position in the xy-plane individually. It is this property which is crucial for the proper operation of convection compensated pulse sequences (*vide infra*). Depending on the tube diameter, sample height, solution viscosity, and density, too strong a temperature gradient can cause the convection to become turbulent. Such convection possesses a chaotic nature, featuring an irregular pattern of flow velocities across the sample. In this case, Eq. [17] does not hold, as v_z is no longer a constant.

To quantitatively describe the effects of diffusion and unidirectional translation on the magnetization during an NMR pulse sequence, the Bloch equations can be modified to account for these effects. Torrey was the first to do this, although only taking diffusion into account (47). The Bloch–Torrey equations, which describe how the magnetization evolves over time under the effects of chemical shift, the inhomogeneous magnetic field along the z-axis, relaxation, unrestricted diffusion, and unidirectional translation, but in the absence of radio frequency (rf) irradiation, are given by

$$\frac{\partial M_Z(t,z)}{\partial t} = \frac{[M_{Z0} - M_z(t,z)]}{T_1} + D\frac{\partial^2 M_Z(t,z)}{\partial z^2} - v_z\frac{\partial M_Z(t,z)}{\partial z}$$

$$\frac{\partial M^{\pm}(t,z)}{\partial t} = \left[\pm i\Omega_0 - \frac{1}{T_2}\right]M^{\pm}(t,z) \mp i\gamma G(t,z)M^{\pm}(t,z)$$

$$+ D\frac{\partial^2 M^{\pm}(t,z)}{\partial z^2} - v_z\frac{\partial M^{\pm}(t,z)}{\partial z}$$

$$[18]$$

with M_Z the longitudinal magnetization, $M^{\pm}$ ($= M_X \pm iM_Y$) the transverse magnetization representing coherence order $p = +1$ or $p = -1$, M_{Z0} the equilibrium magnetization, Ω_0 the chemical shift frequency offset, T_1 and T_2, respectively, the longitudinal and transverse relaxation time constants, γ the gyromagnetic ratio of the nuclear spin, and $G(t,z)$ the time-dependent magnetic field inhomogeneity along the z-axis. The field inhomogeneity along the z-axis creates a time- and z-position-dependent distribution of phase factors in the transverse magnetization. Through the effect of rf-pulses (which for simplicity have not been included in Eq. [18]), transverse magnetization and thus this distribution of phase factors can be transferred to the M_Z magnetization, justifying why also this component of the magnetization in Eq. [18] is labeled as dependent on the variable z. The processes of molecular diffusion and unidirectional translation will spatially rearrange the molecules bearing the nuclear spins, effectively altering the magnetization distribution. This is taken into account by the last two terms in the equations, which are reminiscent of Eqs. [15] and [17].

In a first step, the Bloch–Torrey equations can be simplified by realizing that the effects of chemical shift evolution and relaxation on the magnetization are well-known and are unaffected by the fact that

the magnetization has now become dependent on the variable z. These can therefore be filtered out of Eq. [18] by applying the substitutions

$$M_Z(t,z) = M_{Z0} - [M_{Z0} - \Theta_Z(t,z)]e^{-t/T_1}$$
$$M^\pm(t,z) = \Theta^\pm(t,z)e^{(\pm i\Omega_0 - 1/T_2)t} \qquad [19]$$

which after simplification leads to

$$\frac{\partial \Theta_Z(t,z)}{\partial t} = D\frac{\partial^2 \Theta_Z(t,z)}{\partial z^2} - v_z\frac{\partial \Theta_Z(t,z)}{\partial z}$$
$$\frac{\partial \Theta^\pm(t,z)}{\partial t} = \mp i\gamma G(t,z)\Theta^\pm(t,z) + D\frac{\partial^2 \Theta^\pm(t,z)}{\partial z^2}$$
$$- v_z\frac{\partial \Theta^\pm(t,z)}{\partial z} \qquad [20]$$

Here, the functions $\Theta_Z(t,z)$ and $\Theta^\pm(t,z)$ describe solely the influence of the field inhomogeneity, diffusion, and unidirectional translation on the magnetization and show that we can safely deal with these aspects separately from chemical shift and relaxation.

During a pulse sequence, rf-pulses are applied to convert one type of magnetization into another. Since the Bloch–Torrey equations do not take these rf-pulses into account, we need to know the pathway that will be followed by the magnetization during the entire pulse sequence. Although one pulse sequence can lead to many different pathways, only one is usually selected through rf-pulse phase cycling and/or PFG pulses. This coherence transfer pathway (CTP) describes how the coherence order p varies as a function of time during the pulse sequence. When we incorporate the coherence order as a function of time $p(t)$ into Eq. [20], these can be combined into a single differential equation.

$$\frac{\partial \Theta(t,z)}{\partial t} = -i\gamma p(t)G(t,z)\Theta(t,z) + D\frac{\partial^2 \Theta(t,z)}{\partial z^2} - v_z\frac{\partial \Theta(t,z)}{\partial z}$$
$$[21]$$

Although the Bloch equations, from which we originally began the derivation, only cover evolution of single quantum coherence ($p = \pm 1$) and longitudinal magnetization ($p = 0$), the above equation can also be applied for pulse sequences that include multiple quantum coherence ($|p| > 1$) or zero quantum coherence ($p = 0$) steps in their CTP. In this respect, the equation can be further generalized to cover pulse sequences where the coherence is transferred to nuclei of different gyromagnetic ratios

$$\frac{\partial \Theta(t,z)}{\partial t} = -iP(t)G(t,z)\Theta(t,z) + D\frac{\partial^2 \Theta(t,z)}{\partial z^2} - v_z\frac{\partial \Theta(t,z)}{\partial z}$$
$$[22]$$

with $P(t)$ the sum total of the coherences at each nucleus weighted with their respective gyromagnetic ratio as a function of time, effectively representing the CTP

$$P(t) = \sum_X \gamma_X p_X(t). \qquad [23]$$

PFG NMR experiments usually apply constant magnetic field gradients along the z-axis. For this reason and because the solution to Eq. [22] is not straightforward for non-linear magnetic field inhomogeneities, we will from now on assume that the field inhomogeneities are always linear along the z-axis, but with varying strength over time.

$$G(t,z) = G(t)z \qquad [24]$$

For some NMR probe heads that are not optimally designed for diffusion measurements, this assumption may not always perfectly hold true and significant non-constant z-gradients may be generated by the gradient coils. It can be noted here that in such cases, empirical modifications to the ST equation have been proposed to compensate for deviations of gradient homogeneity (50, 51).

When no diffusion or unidirectional translation were to take place ($D = v_z = 0$), Eq. [22] becomes a simple first order differential equation, with the solution

$$\Theta(t,z) = \Theta(0,z)e^{-izq(t)} \qquad [25]$$

where $q(t)$ is a function that can be interpreted as the amount of dephasing per unit length of the overall magnetization due to the gradients at any point in time.

$$q(t) = \int_0^t P(t)G(t)dt. \qquad [26]$$

Given this result, the solution of Eq. [21] in the presence of diffusion and unidirectional translation can be found by applying the following substitution, which aims to filter out the effects of the field inhomogeneities as was done before for the chemical shift and relaxation

$$\Theta(t,z) = \Phi(t)e^{-izq(t)} \qquad [27]$$

where $\Phi(t)$, the function representing solely the effects of diffusion and unidirectional translation on the magnetization, is here introduced as being dependent only on the variable t, which can be justified as follows. When the magnetic field inhomogeneities are linear, unidirectional translation with constant velocity will have the effect of introducing a phase shift on the mag-

netization that is equal for each position along the z-axis as time progresses. Under the same conditions, diffusion will lead to a loss of magnetization phase coherence at a rate that is constant along the z-axis (Fig. 2). Therefore, when applying only constant magnetic field gradients, the effects of both diffusion and unidirectional translation on the magnetization and thus $\Phi(t)$ will be independent of the position along the z-axis. Substituting Eqs. [24] and [27] into Eq. [22] gives

$$\frac{\partial \Phi(t)}{\partial t}e^{-izq(t)} + \Phi(t)\left[-iz\frac{\partial q(t)}{\partial t}e^{-izq(t)}\right]$$
$$= -izP(t)G(t)\Phi(t)e^{-izq(t)} - D\Phi(t)\left[q^2(t)e^{-izq(t)}\right]$$
$$\quad - v_z\Phi(t)\left[-iq(t)e^{-izq(t)}\right]$$
$$\Leftrightarrow \frac{\partial \Phi(t)}{\partial t} - iz\Phi(t)\frac{\partial q(t)}{\partial t}$$
$$= -izP(t)G(t)\Phi(t) - D\Phi(t)q^2(t) + iv_z\Phi(t)q(t). \quad [28]$$

The derivative of $q(t)$ is found by differentiating Eq. [26], revealing that the last and first term of respectively the left and right sides of Eq. [28] are identical. After simplification, Eq. [28] becomes

$$\frac{\partial \Phi(t)}{\partial t} = \left[-Dq^2(t) + iv_zq(t)\right]\Phi(t). \quad [29]$$

The absence of the variable z confirms the consistency of the above assumption. The solution of this linear differential equation is straightforward, assuming $\Phi(0) = 1$

$$\Phi(t) = e^{-D\int_0^t q^2(t)dt} e^{iv_z\int_0^t q(t)dt}. \quad [30]$$

The equation shows that when diffusion takes place, the magnetization gains a position-independent, exponential attenuation proportional to the diffusion coefficient and the integral over time of the squared amount of dephasing of the overall magnetization per unit length $q^2(t)$. The more strongly the magnetization is dephased (higher $q^2(t)$ function) and the longer the magnetization stays dephased (longer period over which $q^2(t)$ is integrated), the more diffusion will attenuate the magnetization. Note that the integral in the exponent can never become negative and cannot decrease as time progresses, since $q^2(t)$ is at any point a function larger than or equal to zero. This reflects the incoherent and irreversible character of diffusion and thus of the magnetization coherence loss. On the other hand, the effect of unidirectional translation is to introduce a position independent phase shift proportional to

the translation velocity and the integral over time of $q(t)$. Since the translation is a coherent process, as all molecules move in the same direction at the same velocity, the effects on the magnetization are reversible. Indeed, the function $q(t)$ can be positive or negative, allowing its integral to either increase or decrease with time. The implication of this is that by proper choice of the $q(t)$ function, i.e., the gradient strength as a function of time and the CTP, the integral over this function can cross zero, so that at that point there is no net phase shift due to the translation, irrespective of the value of v_z. This principle is exploited in convection-compensated pulse sequences (*vide infra*).

Note that in the Bloch–Torrey equations, it was inherently assumed that the distances over which the molecules diffuse or translate during the experiment time considered are much smaller than the dimensions of the sample or than the space the molecules are confined in. In the opposite case, diffusion would not be free and restricted diffusion would need to be considered. In addition, this derivation assumes that the phase dispersion generated by the gradient pulses is sufficient to make the net resultant signal negligible.

To find the impact of diffusion and unidirectional translation on pulse sequences, Eq. [30] must be evaluated. The procedure to do this occurs in three steps. First, the gradient strength evolution over time (the "gradient pattern") and the CTP of the pulse sequence must be identified so that the functions $G(t)$ and $P(t)$ are defined. Second, the $q(t)$ function as defined in Eq. [26] must be evaluated over the entire pulse sequence. Finally, integration of the $q(t)$ and $q^2(t)$ functions over the entire duration of the pulse sequence t_{tot} will lead to the full expression for the attenuation due to diffusion E_{diff}, effectively the ST equation, and the phase factor induced by unidirectional translation, E_{transl}

$$\Phi(t_{tot}) = E_{diff}E_{transl} = \underbrace{e^{-D\int_0^{t_{tot}} q^2(t)dt}}_{E_{diff}}\underbrace{e^{iv_z\int_0^{t_{tot}} q(t)dt}}_{E_{transl}}. \quad [31]$$

In what follows, this will be illustrated for several pulse sequences that are designed for measuring diffusion.

BASIC PFG PULSE SEQUENCES TO MEASURE DIFFUSION

The Basic PFG Experiment: Monopolar Gradients

Stejskal and Tanner (*33*) were the first to apply the concept of diffusional signal attenuation as a fully
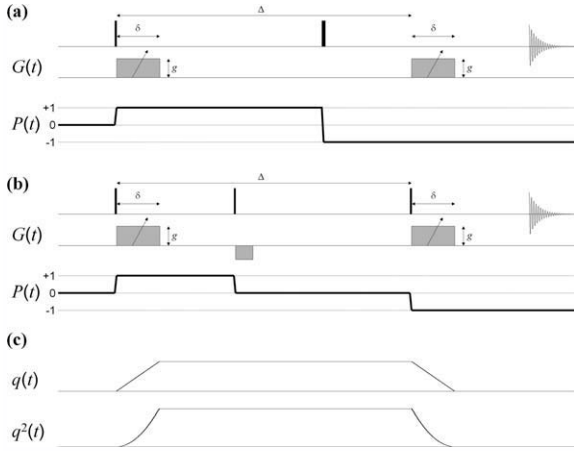
Figure 3 Spin or Hahn echo (a) and STE sequences (b), with CTP function $P(t)$, $q(t)$, and $q^2(t)$ functions.

developed method to measure diffusion coefficients. Instead of using steady gradients that are active during the whole of the spin-echo experiment, they described the advantages of applying time-dependent, PFGs [Fig. 3(a)]. Using the Bloch–Torrey equations, they derived the diffusion attenuation for their spin-echo experiment, which is widely known today as the ST equation. They also introduced the convention of labeling the delays in a PFG pulse sequence. The length of the diffusion encoding and decoding gradient pulses and the time between the start of both these gradients are labeled δ and Δ, respectively, while the maximum strength of the gradient pulses is given by g (Fig. 3). Because the diffusion and translation encoding and decoding gradient pulses are a single gradient pulse, this set-up is also referred to as applying monopolar gradient pulses.

The gradient strength function $G(t)$ and the coherence order pathway $P(t)$ for the spin-echo sequence are illustrated in Fig. 3(a). Their product is given by

$$P(t)G(t) = \begin{cases} \gamma g a(t) & 0 \le t \le \delta \\ 0 & \delta \le t \le \Delta \\ -\gamma g a(t - \Delta) & \Delta \le t \le \Delta + \delta \end{cases} \quad . \quad [32]$$

Here, $a(t)$ represents the shape of the PFG pulses covering the pulse length δ. Its relation to the shape function $s(t)$ from Table 1 is

$$a(t) = s(t/\delta) \qquad [33]$$

which can be substituted into Eq. [32]

$$P(t)G(t) = \begin{cases} \gamma g s(t/\delta) & 0 \le t \le \delta \\ 0 & \delta \le t \le \Delta \\ -\gamma g s([t - \Delta]/\delta) & \Delta \le t \le \Delta + \delta \end{cases} \quad .$$

$$[34]$$

From Eq. [12], the following is found

$$\int_{t_0}^{t} s([t - t_0]/\delta)dt = \delta \int_{0}^{[t-t_0]/\delta} s([t - t_0]/\delta)d([t - t_0]/\delta)$$

$$= \delta S([t - t_0]/\delta).$$

$$[35]$$

The function $q(t)$ is then, according to Eq. [26] and the definition of the gradient shape factor σ in Eq. [9]

$$q(t) = \begin{cases} \gamma \delta g S(t/\delta) & 0 \le t \le \delta \\ \gamma \delta g \sigma & \delta \le t \le \Delta \\ \gamma \delta g [\sigma - S([t - \Delta]/\delta)] & \Delta \le t \le \Delta + \delta \end{cases} \quad .$$

$$[36]$$

The square of $q(t)$ is

$$q^2(t) = \begin{cases} \gamma^2 \delta^2 g^2 S^2(t/\delta) & 0 \le t \le \delta \\ \gamma^2 \delta^2 g^2 \sigma^2 & \delta \le t \le \Delta \\ \gamma^2 \delta^2 g^2 \sigma^2 + S^2([t - \Delta]/\delta) & \Delta \le t \le \Delta + \delta \\ \quad -2\sigma S([t - \Delta]/\delta)] \end{cases}$$

$$[37]$$

To evaluate the integral of $q(t)$ and $q^2(t)$ over the entire pulse sequence, the previously defined gradient shape parameters λ (Eq. [10]) and κ (Eq. [11]) are introduced at this point

$$\int_{t_0}^{t_0+\delta} S([t - t_0]/\delta)dt = \int_{0}^{\delta} S(t/\delta)dt = \delta \int_{0}^{1} S(t/\delta)d(t/\delta) = \delta\sigma\lambda$$

$$[38]$$

$$\int_{t_0}^{t_0+\delta} S^2([t - t_0]/\delta)dt = \int_{0}^{\delta} S^2(t/\delta)dt = \delta \int_{0}^{1} S^2(t/\delta)d(t/\delta) = \delta\sigma^2\kappa.$$

$$[39]$$

The integral of $q(t)$, required to assess the effects of unidirectional translation, is then evaluated as

$$\ln(E_{\text{transl}}) = \int_0^{\Delta+\delta} q(t)dt$$

$$= \gamma\delta g \left[\underbrace{(\delta\sigma\lambda)}_{0 \leq t \leq \delta} + \underbrace{(\Delta-\delta)\sigma}_{\delta \leq t \leq \Delta} + \underbrace{(\delta\sigma - \delta\sigma\lambda)}_{\Delta \leq t \leq \Delta+\delta} \right]$$

$$= \gamma\delta\sigma g\Delta \qquad [40]$$

Similarly, the integral of $q^2(t)$, to assess the effects of diffusion, is evaluated as

$$\ln(E_{\text{diff}}) = \int_0^{\Delta+\delta} q^2(t)dt = \gamma^2\delta^2 g^2$$

$$\times \left[\underbrace{(\delta\sigma^2\kappa)}_{0 \leq t \leq \delta} + \underbrace{(\Delta-\delta)\sigma^2}_{\delta \leq t \leq \Delta} + \underbrace{(\delta\sigma^2 + \delta\sigma^2\kappa - 2\delta\sigma^2\lambda)}_{\Delta \leq t \leq \Delta+\delta} \right]$$

$$= \gamma^2\delta^2\sigma^2 g^2[\Delta + 2(\kappa-\lambda)\delta] \qquad [41]$$

The only thing at this point that is still undetermined is the shape of the gradient pulses, which defines the values of σ, κ, and λ. For example, when the shape is rectangular, according to Table 1 the complete ST equation becomes

$$E_{\text{diff}} = e^{-D\gamma^2\delta^2 g^2 \left(\Delta - \frac{\delta}{3}\right)}. \qquad [42]$$

On the other hand, for sine bell shaped gradient pulses, the ST equation becomes

$$E_{\text{diff}} = e^{-D\gamma^2\delta^2 \frac{4}{\pi^2} g^2 \left(\Delta - \frac{\delta}{4}\right)}. \qquad [43]$$

This derivation of the ST equation is applicable not only to the spin-echo sequence, but equally well to any pulse sequence that follows the same pattern of monopolar encoding and decoding gradient pulses. Deviations occur when there is either a constant background z-gradient present (52) (i.e., an inhomogeneous static magnetic field) or when additional gradient pulses for CTP selection between the encoding and decoding gradient pulses are present (*vide infra*), except when the desired CTP during such gradient has zero coherence order.
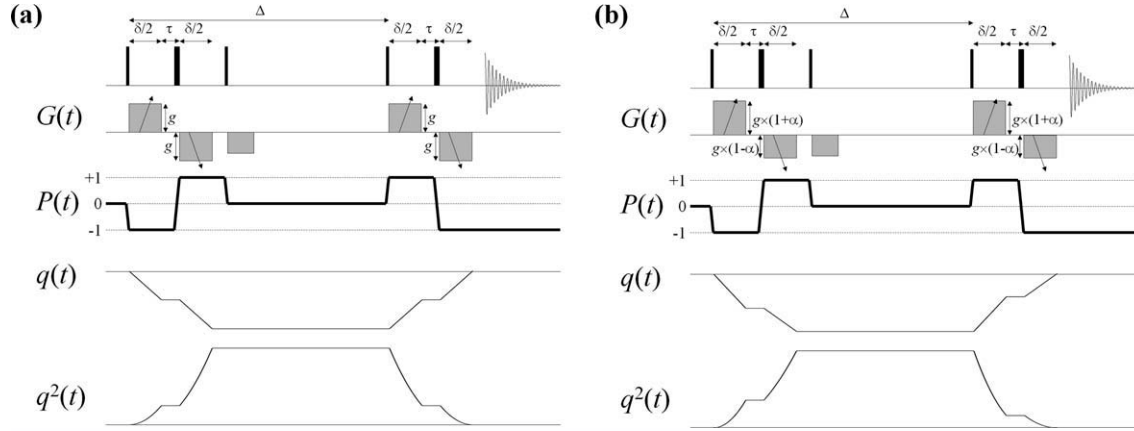
One example is the stimulated echo (STE) sequence [Fig. 3(b)], first investigated by Hahn (43) and later introduced for diffusion measurements by Tanner (53). In a STE, the chemical shift is refocused by two 90° pulses instead of one 180° pulse. Between these two gradients, there typically exists a spoiler gradient pulse to assist in selecting the correct CTP, but since the coherence order selected during this pulse is zero, it does not affect the ST equation. The advantage of the STE sequence is that the magnetization is stored longitudinally during most of the diffusion delay time Δ, which can be several hundreds of milliseconds long. In this way, peak distortions in the spectrum due to scalar coupling evolution during the pulse sequence will be significantly reduced. Also, signal loss due to relaxation is much reduced for large molecular entities for which longitudinal relaxation is significantly less efficient than transverse relaxation. Opposed to this is an inherent loss in signal by a factor of two compared to the spin-echo sequence, since only half of the magnetization (dephased due to the gradient) can be transferred to the longitudinal axis by the 90° pulse. However, for large molecules, this is typically more than compensated for by the relaxation advantage. One last disadvantage is that the extra rf-pulse in the sequence will require more phase cycling and thus a higher number of minimum transients to select the correct CTP. All together, in most cases the STE sequence appears to be more advantageous and therefore more widely used than the spin echo.

Pulse Sequences Applying Bipolar Gradient Pulses

A common modification to PFG diffusion experiments is the implementation of bipolar gradient pulses. In this set-up, instead of a single (monopolar) gradient pulse with duration δ, a pair of gradient pulses of equal duration $\delta/2$ and opposite sign is used with a 180° rf-pulse positioned in between (Fig. 4) (54, 55). The 180° pulse inverts the sign of the coherence order p, so that the second gradient pulse continues the dephasing started by the first one. The product of the gradient strength function $G(t)$ with the coherence order pathway $P(t)$ is given by

$$P(t)G(t)$$
$$= \begin{cases} -\gamma gb(t) & 0 \leq t \leq \delta/2 \\ 0 & \delta/2 \leq t \leq \delta/2 + \tau \\ -\gamma gb(t - \delta/2 - \tau) & \delta/2 + \tau \leq t \leq \delta + \tau \\ 0 & \delta + \tau \leq t \leq \Delta \\ \gamma gb(t - \Delta) & \Delta \leq t \leq \Delta + \delta/2 \\ 0 & \Delta + \delta/2 \leq t \leq \Delta + \delta/2 + \tau \\ \gamma gb(t - \Delta - \delta/2 - \tau) & \Delta + \delta/2 + \tau \leq t \leq \Delta + \delta + \tau \end{cases}$$

$$[44]$$

Figure 4 STE sequence applying symmetrical bipolar gradient pulses (a) and one-shot pulse sequence applying assymetrical bipolar gradient pulses (b), with CTP function $P(t)$, $q(t)$, and $q^2(t)$ functions.

where $b(t)$ represents the gradient shape of the individual gradient pulses within the bipolar gradient. The constant τ is the total delay between these gradient pulses, which represents the duration of the gradient recovery delay and the 180° pulse. The functions $b(t)$ are similar to the monopolar gradient shapes $a(t)$, except that these occur over a time $\delta/2$ instead of δ. The relation between $b(t)$ and the shape functions $s(t)$ defined in Table 1 is

$$b(t) = s(2t/\delta) \qquad [45]$$

which can be substituted into Eq. [44]

$$P(t)G(t)$$

$$= \begin{cases} -\gamma g s(2t/\delta) & 0 \leq t \leq \delta/2 \\ 0 & \delta/2 \leq t \leq \delta/2 + \tau \\ -\gamma g s(2[t - \delta/2 - \tau]/\delta) & \delta/2 + \tau \leq t \leq \delta + \tau \\ 0 & \delta + \tau \leq t \leq \Delta \\ \gamma g s(2[t - \Delta]/\delta) & \Delta \leq t \leq \Delta + \delta/2 \\ 0 & \Delta + \delta/2 \leq t \leq \Delta + \delta/2 + \tau \\ \gamma g s(2[t - \Delta - \delta/2 - \tau]/2 - \tau]\delta\delta) & \Delta + \delta/2 + \tau \leq t \leq \Delta + \delta + \tau \end{cases}$$

$$[46]$$

From Eq. [12], the following is found

$$\int_{t_0}^{t} s(2[t-t_0]/\delta)dt = \frac{\delta}{2} \int_{0}^{2[t-t_0]/\delta} s(2[t-t_0]/\delta)d(2[t-t_0]/\delta)$$

$$= \frac{\delta}{2}S(2[t-t_0]/\delta).$$

$$[47]$$

The function $q(t)$ is then, according to Eq. [26] and the definition of the gradient shape factor σ in Eq. [9]

$$q(t) = \begin{cases} -\gamma\frac{\delta}{2}gS(2t/\delta) & 0 \leq t \leq \delta/2 \\ -\gamma\frac{\delta}{2}g\sigma & \delta/2 \leq t \leq \delta/2 + \tau \\ -\gamma\frac{\delta}{2}g[\sigma + S(2[t - \delta/2 - \tau]/2 - \tau]/\delta)] & \delta/2 + \tau \leq t \leq \delta + \tau \\ -\gamma\delta g\sigma & \delta + \tau \leq t \leq \Delta \\ \gamma\frac{\delta}{2}g[-2\sigma + S(2[t - \Delta]/\delta)] & \Delta \leq t \leq \Delta + \delta/2 \\ -\gamma\frac{\delta}{2}g & \sigma\Delta + \delta/2 \leq t \leq \Delta + \delta/2 + \tau \\ \gamma\frac{\delta}{2}g[-\sigma + S(2[t - \Delta - \delta/2 - \tau]/2 - \tau]/\delta)] & \Delta + \delta/2 + \tau \leq t \leq \Delta + \delta + \tau \end{cases} \quad . \quad [48]$$

The square of $q(t)$ is

$$
q^2(t) = \begin{cases}
\gamma^2 \dfrac{\delta^2}{4} g^2 S^2(2t/\delta) & 0 \leq t \leq \delta/2 \\[2ex]
\gamma^2 \dfrac{\delta^2}{4} g^2 \sigma^2 & \delta/2 \leq t \leq \delta/2 + \tau \\[2ex]
\gamma^2 \dfrac{\delta^2}{4} g^2 \left[\sigma^2 + S^2(2[t - \delta/2 - \tau]\delta) + 2\sigma S(2[t - \delta/2 - \tau]/\delta)\right] & \delta/2 + \tau \leq t \leq \delta + \tau \\[2ex]
\gamma^2 \delta^2 g^2 \sigma^2 & \delta + \tau \leq t \leq \Delta \\[2ex]
\gamma^2 \dfrac{\delta^2}{4} g^2 \left[4\sigma^2 + S^2(2[t - \Delta]/\delta) - 4\sigma S(2[t - \Delta]/\delta)\right] & \Delta \leq t \leq \Delta + \delta/2 \\[2ex]
\gamma^2 \dfrac{\delta^2}{4} g^2 \sigma^2 & \Delta + \delta/2 \leq t \leq \Delta + \delta/2 + \tau \\[2ex]
\gamma^2 \dfrac{\delta^2}{4} g^2 [\sigma^2 + S^2(2[t - \Delta - \delta/2]/\delta) & \Delta + \delta/2 + \tau \leq t \leq \Delta + \delta + \tau \\
\quad - 2\sigma S(2[t - \Delta - \delta/2 - \tau]/\delta)] &
\end{cases}
\tag{49}
$$

Similarly as for monopolar gradients, the following integrals can be related with λ (Eq. [10]) and κ (Eq. [11])

$$
\int_{t_0}^{t_0+\delta/2} S(2[t - t_0]/\delta)dt = \frac{\delta}{2}\sigma\lambda \tag{50}
$$

$$
\int_{t_0}^{t_0+\delta/2} S^2(2[t - t_0]/\delta)dt = \frac{\delta}{2}\sigma^2\kappa. \tag{51}
$$

Applying these relations, the evaluation of the integral of $q(t)$ over the entire pulse sequence, is

$$
\ln(E_{\text{transl}}) = \int_0^{\Delta+\delta+\tau} q(t)dt
$$

$$
= -\gamma\frac{\delta}{2}g\left[\underbrace{\left(\frac{\delta\sigma\lambda}{2}\right)}_{0\leq t\leq\delta/2} + \underbrace{(\sigma\tau)}_{\delta/2\leq t\leq\delta/2+\tau} + \underbrace{\left(\frac{\delta}{2}\sigma + \frac{\delta\sigma\lambda}{2}\right)}_{\delta/2+\tau\leq t\leq\delta+\tau} + \underbrace{2\sigma(\Delta - \delta - \tau)}_{\delta+\tau\leq t\leq\Delta}\right.
$$

$$
\left. + \underbrace{\left(\delta\sigma - \frac{\delta\sigma\lambda}{2}\right)}_{\Delta\leq t\leq\Delta+\delta/2} + \underbrace{(\sigma\tau)}_{\Delta+\delta/2\leq t\leq\Delta+\delta/2+\tau} + \underbrace{\left(\frac{\delta\sigma}{2} - \frac{\delta\sigma\lambda}{2}\right)}_{\Delta+\delta/2+\tau\leq t\leq\Delta+\delta+\tau}\right]
$$

$$
= -\gamma\delta\sigma g\Delta \tag{52}
$$

which is the same result as in the case of monopolar gradients (Eq. [40]) apart from the negative sign. The integral of $q^2(t)$ is evaluated as

$$
\ln(E_{\text{diff}}) = \int_0^{\Delta+\delta+\tau} q^2(t)dt
$$

$$
= \gamma^2\frac{\delta^2}{4}g^2\left[\underbrace{\left(\frac{\delta\sigma^2\kappa}{2}\right)}_{0\leq t\leq\delta/2} + \underbrace{(\sigma^2\tau)}_{\delta/2\leq t\leq\delta/2+\tau} + \underbrace{\left(\frac{\delta\sigma^2}{2} + \frac{\delta\sigma^2\kappa}{2} + \delta\sigma^2\lambda\right)}_{\delta/2+\tau\leq t\leq\delta+\tau}\right.
$$

$$
+ \underbrace{4\sigma^2(\Delta - \delta - \tau)}_{\delta+\tau\leq t\leq\Delta} + \underbrace{\left(2\delta\sigma^2 + \frac{\delta\sigma^2\kappa}{2} - 2\delta\sigma^2\lambda\right)}_{\Delta\leq t\leq\Delta+\delta/2}
$$

$$
+ \underbrace{(\sigma^2\tau)}_{\Delta+\delta/2\leq t\leq\Delta+\delta/2+\tau} + \left.\underbrace{\left(\frac{\delta\sigma^2}{2} + \frac{\delta\sigma^2\kappa}{2} - \delta\sigma^2\lambda\right)}_{\Delta+\delta/2+\tau\leq t\leq\Delta+\delta+\tau}\right]
$$

$$
= \gamma^2\delta^2\sigma^2 g^2\left[\Delta + \frac{(2\kappa - 2\lambda - 1)\delta}{4} - \frac{\tau}{2}\right] \tag{53}
$$

This result is clearly different from the one obtained in Eq. [41] for monopolar gradient sequences.

There are some interesting advantages to the bipolar gradient set-up. The implementation of two gradient pulses with opposite sign in immediate succession will have a much reduced effect on the deuterium lock signal. Since the deuterium magnetization is also dephased by the gradient pulse, the lock signal will momentarily disappear until it has recovered through relaxation. During this time, the field lock cannot be applied, possibly leading to frequency shift artifacts. With bipo-
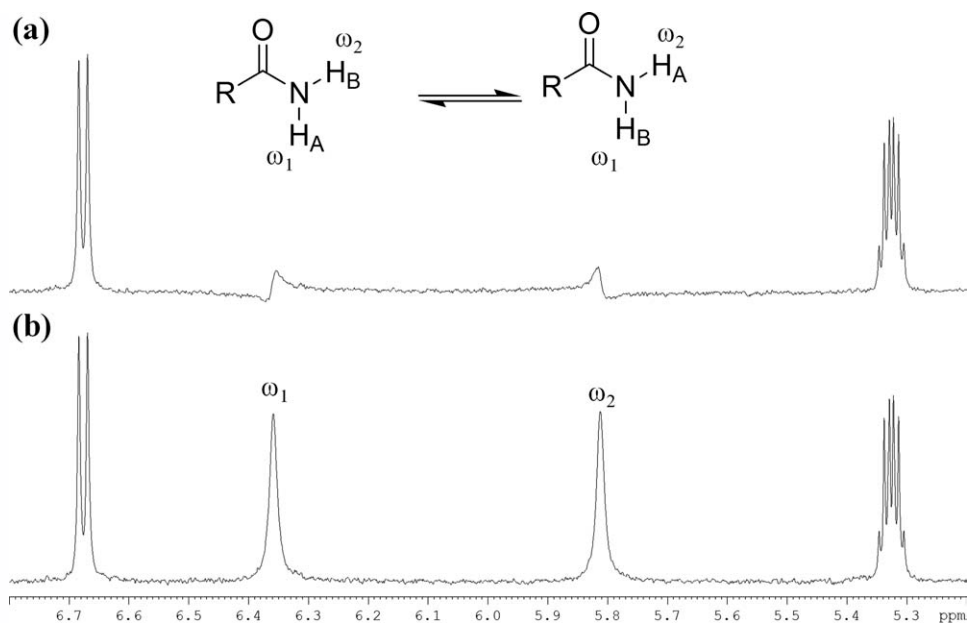
Figure 5 Illustration of the effect of exchange on the signal phase in an STE experiment. The two central resonances represent the two protons of the $CONH_2$ group of a glutamine residue in the cyclic lipodepsipeptide pseudodesmin A (*57*) in acetonitrile solution measured at 25°C and 16.4 T, which are in slow exchange on the frequency time scale. (a) Monopolar gradient STE experiment, demonstrating that the exchange is sufficiently fast so that it occurs during the diffusion delay Δ. Note the exactly opposite phase distortion of both residual peaks. The time U between the first two 90° pulses is 1.45 ms, while the frequency difference between both peaks is 383 Hz, leading to a phase factor of 200° according to Eq. [55]. This explains the reduced signal intensity, as the fraction that has exchanged contributes to the signal with an opposite sign compared to the fraction that has not exchanged, i.e., the phase factor is close to 180°. (b) Bipolar gradient STE with exactly the same Δ and δ durations. The phase distortion is no longer present and the signal intensity has been restored, showing that the exchange is too slow to significantly occur during the much shorter delay U. The multiplet at 5.32 ppm and the doublet at 6.68 ppm are not involved in any exchange process and are thus invariable between both pulse sequences.

lar gradients, the deuterium signal will be immediately refocused by the second gradient, since it is of course does not experience the effect of the 180° pulse at the frequency of the nucleus of interest.

A second notable advantage arises when slow chemical exchange processes on the frequency time scale exist during an STE experiment (*56*). Assume that a nucleus exchanges between two sites 1 and 2 where it resonates at different frequencies ω_1 and ω_2. If during the delay between the first two 90° pulses of a monopolar gradient STE experiment [Fig. 3(b)], the nucleus is at site 1, then a phase factor will develop through chemical shift evolution (ignoring the effects of the gradient for simplicity)

$$M^+ \xrightarrow{\omega_1 M_Z U} M^+ e^{-i\omega_1 U} \qquad [54]$$

with U the time between the first two 90° pulses, usually on the order of δ. If at some point during the much longer delay between the second and third pulses—on the order of Δ—the nucleus exchanges from site 1 to site 2, the chemical shift evolution during the time U after the third 90° pulse and before the start of the acquisition will be

$$M^- e^{-i\omega_1 U} \xrightarrow{\omega_2 M_Z U} M^- e^{i(\omega_2 - \omega_1)U}. \qquad [55]$$

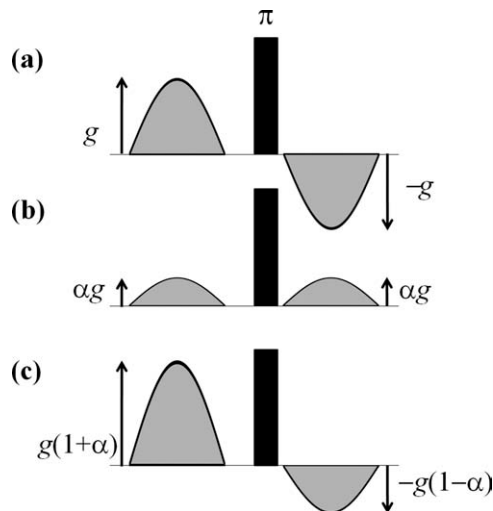Since in general ω_1 and ω_2 are not equal, it is clear that the phase factors that develop between both delays will not vanish. If the exchange rate is such that a significant fraction of nuclei exchange between the sites during the delay, this fraction will possess this phase factor as opposed to the fraction that did not exchange, leading to peak distortions (*56*). When using bipolar PFGs, the 180°

pulse acts as a spin echo, refocusing the chemical shift evolution during the time U. Thus the time interval during which chemical exchange would need to occur in order for a chemical shift phase factor to develop is much shorter in the bipolar gradient experiment (U) than in the monopolar gradient experiment ($U + \Delta$). Therefore, the bipolar gradient STE sequence offers a significant advantage when studying systems undergoing slow exchange. An example that nicely illustrates this is shown in Fig. 5.

The disadvantage is that again more rf-pulses are added to the sequence, requiring a more extended phase cycling to correct for imperfect 180° pulses. A proposed solution for this issue is the introduction of asymmetric or unbalanced bipolar gradient pulses (58) [Fig. 4(b)]. These can be regarded as the sum (or the difference) of a symmetric bipolar gradient pulse and two gradient pulses that select for the inversion of coherence order ($p \rightarrow -p$) in a spin echo (Fig. 6). In principle, this eliminates the need for phase cycling the 180° pulses, even allowing the full pulse sequence to run with a single scan. In this pulse sequence, known as the one-shot sequence (58), the relative contribution α of the CTP selection gradient pulses to the total unbalanced gradient pulses is chosen as fixed, i.e., as gradient strength αg. When g is small however—i.e., in the first increments of the diffusion experiment—the unwanted magnetization might be insufficiently suppressed, leading to an additional contribution to the signal intensity that drops as g increases and thus to an additional attenuation that will be confounded with the diffusion attenuation. This effectively results in overestimated diffusion coefficients. When this effect is quite strong due to imperfect rf-pulse calibration or B_1-field inhomogeneity, a short phase cycle can be reintroduced to alleviate this problem.

The product of the gradient strength function $G(t)$ with the coherence order pathway $P(t)$ for the one-shot sequence is given by

$$P(t)G(t)$$

$$= \begin{cases} -\gamma g(1+\alpha)b(t) & 0 \leq t \leq \delta/2 \\ 0 & \delta/2 \leq t \leq \delta/2 + \tau \\ -\gamma g(1-\alpha)b(t-\delta/2-\tau) & \delta/2 + \tau \leq t \leq \delta + \tau \\ 0 & \delta + \tau \leq t \leq \Delta \\ \gamma(1+m\alpha)gb(t-\Delta) & \Delta \leq t \leq \Delta + \delta/2 \\ 0 & \Delta + \delta/2 \leq t \leq \Delta + \delta/2 + \tau \\ \gamma(1-m\alpha)gb(t-\Delta-\delta/2-\tau) & \Delta + \delta/2 + \tau \leq t \leq \Delta + \delta + \tau \end{cases}$$

$$[56]$$

Figure 6 (a) The symmetrical bipolar gradient pulse consists out of two gradients with opposite polarity at each side of the 180° pulse. Both gradient pulses will add up in the dephasing of the magnetization, but will not contribute to the CTP selection of the pulse sequence, leaving the need for phase cycling of the rf-pulses. (b) Gradients of equal polarity at each side of the 180° pulse will select all CTPs where the coherence order after the 180° pulse is the additive inverse of that before the pulse, but will ultimately not provide a contribution to the $q(t)$ function. (c) Addition of both gradient patterns creates an asymmetrical bipolar gradient pulse, introducing CTP selectivity while retaining magnetization dephasing.

Here, m is a constant representing the ratio of the unbalancing factors of the first and second bipolar gradient pulses. In the original one-shot-sequence (58), only values of m equal to $+1$ or -1 were considered, although in principle any value could be considered. The integral of the $q^2(t)$ and $q(t)$ functions can be derived just as before, with the final results given by

$$\ln(E_{\text{diff}}) = \int_0^{\Delta+\delta+\tau} q^2(t)dt$$

$$= \gamma^2\delta^2\sigma^2 g^2 \left[\Delta + \frac{(\kappa-\lambda)(\alpha^2(1+m^2)+2)\delta}{4}\right.$$

$$\left. + \frac{(\delta+2\tau)}{8}\left(\alpha^2\left(1+m^2\right)+2\alpha(1-m)-2\right)\right] \quad [57]$$

$$\ln(E_{\text{transl}}) = \int_0^{\Delta+\delta+\tau} q(t)dt = -\gamma\delta\sigma g\left[\Delta + \alpha(1-m)\left(\frac{\delta}{2}+\tau\right)\right].$$

$$[58]$$

Convection Compensated Pulse Sequences

As discussed before, convection cells in the NMR tube are often induced by temperature gradients arising from the heated air flow in the probe necessary for temperature control. In the middle of the sample, the convection cell can be regarded as several fluid flows nearly parallel to the z-axis, each with a constant flow velocity v_z. Because there is a distribution of these flow velocities, a distribution of phase factors will develop for the total magnetization under the influence of the magnetic field inhomogeneities. To illustrate this, assume a simple uniform velocity distribution (*49*) ranging between $-v_z^{\max}$ and $+v_z^{\max}$ (see the article by Jerschow (*48*) for a more realistic velocity distribution) during one of the diffusion experiments described above. The total signal attenuation due to convection E_{conv} will be the average of the phase factors:

$$E_{\mathrm{conv}} = \frac{1}{2v_z^{\max}} \int_{-v_z^{\max}}^{v_z^{\max}} E_{\mathrm{transl}}(v_z)dv_z$$

$$= \frac{1}{2v_z^{\max}} \int_{-v_z^{\max}}^{v_z^{\max}} e^{iv_z\gamma\delta\sigma g\Delta}dv_z = \frac{e^{iv_z^{\max}\gamma\delta\sigma g\Delta} - e^{-iv_z^{\max}\gamma\delta\sigma g\Delta}}{2iv_z^{\max}\gamma\delta\sigma g\Delta}$$

$$= \mathrm{sinc}\left(v_z^{\max}\gamma\delta\sigma g\Delta\right) \quad [59]$$

with Δ the diffusion delay (assuming no correction term). In the presence of convection, the signal intensity will evolve as a sinc function with increasing gradient strength g, which is a damped oscillation. When it is the purpose of the experiment to measure the diffusion coefficient, the presence of convection will disrupt the signal attenuation due to diffusion, making it impossible to accurately determine the diffusion coefficient. For this reason, whether convection is present or not is a very important question to address when setting up diffusion measurements.

NMR experiments have been described to detect the presence of convection (*49*). However, when not explicitly looking for convection, the quickest way to unambiguously detect its presence is by observing a change in sign for the signal intensity when increasing g during a diffusion NMR experiment due to the nature of the sinc function. This is often the case in low viscosity solvents, such as chloroform. However, convection is most troublesome when it is present to a very low extent so that $v_z^{\max}\gamma g\delta\sigma\Delta$ is small, since then the sinc decay is not easy to differentiate from a Gaussian decay. This is shown by applying the trun-cated Maclaurin series expansions of the sine and exponential functions

$$\frac{\sin\left(v_z^{\max}\gamma\delta\sigma g\Delta\right)}{v_z^{\max}\gamma\delta\sigma g\Delta} \approx \frac{v_z^{\max}\gamma\delta\sigma g\Delta - \frac{\left(v_z^{\max}\gamma\delta\sigma g\Delta\right)^3}{6}}{v_z^{\max}\gamma\delta\sigma g\Delta}$$

$$= 1 - \frac{\left(v_z^{\max}\gamma\delta\sigma g\Delta\right)^2}{6} \approx e^{-\frac{\left(v_z^{\max}\gamma\delta\sigma g\Delta\right)^2}{\sqrt{6}}} \quad [60]$$

This can be combined with the ST equation for diffusion, assuming the approximation that $\Delta' \approx \Delta$

$$E_{\mathrm{tot}} = E_{\mathrm{diff}}E_{\mathrm{conv}} = e^{-D\gamma^2\delta^2\sigma^2 g^2\Delta'}e^{-\frac{\left(v_z^{\max}\gamma\delta\sigma g\Delta\right)^2}{\sqrt{6}}}$$

$$\approx e^{-\left(D+\frac{(v_z^{\max})^2\Delta}{\sqrt{6}}\right)\gamma^2\delta^2\sigma^2 g^2\Delta'}. \quad [61]$$

This result is by no means meant to describe the total signal attenuation E_{tot} due to both diffusion and convection, as it is based on several approximations. However, it does illustrate that when limited convection is present, the total attenuation will be close to that of the Gaussian functional form as would have been expected when only taking diffusion into account, masking the convection's presence (*59*). The apparent diffusion coefficient will be increased by an amount proportional to both the square of the convection velocity and the diffusion delay Δ. Therefore, the unsuspecting experimentalist can significantly overestimate the diffusion coefficient, especially for slowly diffusing species at long diffusion delays. If the purpose of the diffusion experiment is simply to make a distinction between components with strongly differing diffusion coefficients by use of a 2D DOSY plot, a slight convection effect may be acceptable. However, when it is the absolute value of the diffusion coefficient as a physical quantity that is desired, or when D as a function of Δ is studied for the purpose of studying chemical exchange for example (*6, 19, 20*), the effects of convection must be minimized.

Convection can be reduced or avoided by limiting the sample filling height to the absolute minimum, decreasing the sample diameter or, if feasible, by using solvents with higher viscosity or density. Another possibility is to simply disconnect the temperature control unit from the spectrometer to avoid temperature gradients forming along the sample. The obvious disadvantage of this is that the temperature cannot be properly set and stabilized under these conditions. Also, the indirect heating of the sample during the PFG experiment caused by the Joule effect from the electrical currents through the gradient coils
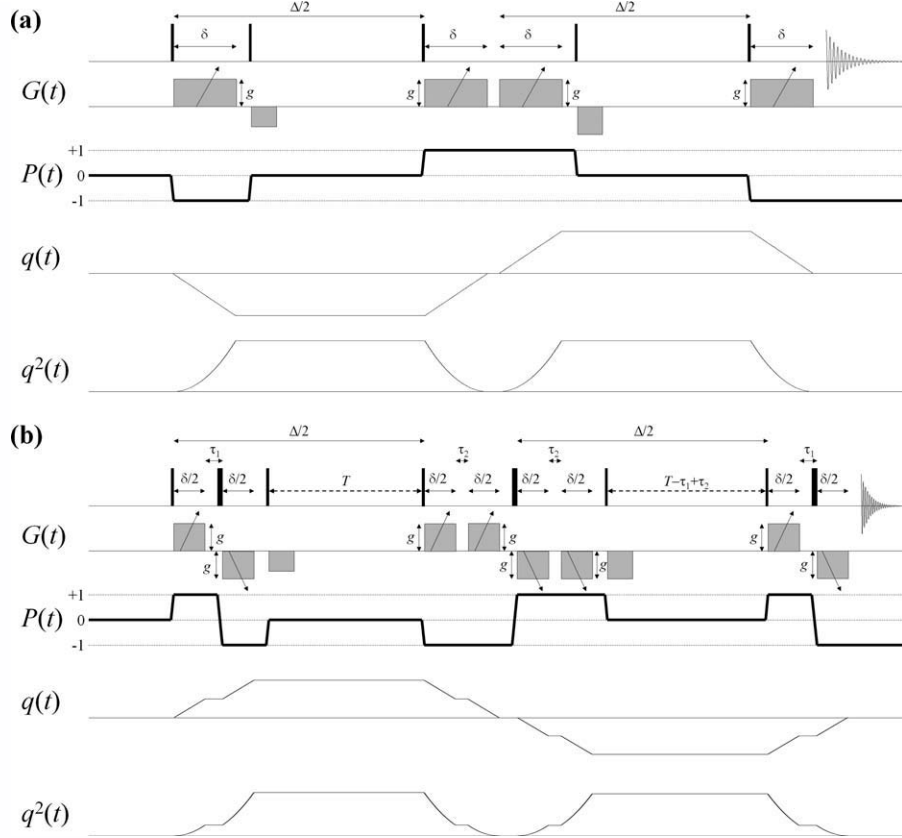
Figure 7 Pulse sequences for convection compensation, with CTP function $P(t)$, $q(t)$, and $q^2(t)$. (a) Double STE sequence, applying monopolar gradient pulses. (b) Double STE sequence, applying bipolar gradient pulses. Note the two separately defined intergradient delays within the bipolar gradient pulses, τ_1 and τ_2. The sequence as shown here assumes equal diffusion delays $\Delta/2$ for both STEs, necessarily leading to unequal delays between the $90°$ pulses, T and $T-\tau_1+\tau_2$ respectively.

will not be properly compensated for, resulting in increased sample temperature as the gradient strength increases.

A more elegant solution is to apply convection compensated pulse sequences, as proposed by Jerschow and Muller (*60*). These techniques are based on the principle that the function $q(t)$ can switch its sign during the pulse sequence, so that its integral and thus the effects of unidirectional translation and flow at one specific point will vanish. To demonstrate this approach, consider the pulse sequence in Fig. 7(a). It consists of two subsequent STE sequences (double STE or dSTE), each with a diffusion delay of $\Delta/2$. The only difference is that their CTPs are exactly opposite in sign. The consequence of this is that their $q(t)$ functions are equal in magnitude but also opposite in sign. When assuming v_z remains constant during and between both STEs and across a distance that is larger than the translation displacement, the total phase factor developed at the

end of the pulse sequence due to the translation is the product of the phase factors of each individual STE sequence, which consequently cancel each other out

$$E_{\text{transl}} = e^{iv_z \int_{\text{STE1}} q(t)dt} \times e^{-iv_z \int_{\text{STE2}} q(t)dt} = 1. \quad [62]$$

On the other hand, the attenuation due to diffusion is dependent on the $q^2(t)$ function, which is equal for both STE parts. The net diffusion attenuation is thus the square of the attenuation of a single STE sequence

$$E_{\text{diff}} = e^{-D \int_{\text{STE1}} q^2(t)dt} \times e^{-D \int_{\text{STE2}} q^2(t)dt} = e^{-2D \int_{\text{STE}} q^2(t)dt}. \quad [63]$$

Using the result of Eq. [41] of a single STE sequence, now with diffusion delay $\Delta/2$ yields

$$E_{\text{diff}} = e^{-2D \int_0^{\frac{\Delta}{2}+\delta} q^2(t)dt} = e^{-D\gamma^2\delta^2\sigma^2 g^2[\Delta+4\kappa-4\lambda]}. \quad [64]$$

The choice of a diffusion delay of $\Delta/2$ for each diffusion encoding/decoding segment allows for easy comparison with the non-convection compensated equivalent pulse sequences, differing then only in the correction term to Δ in the attenuation equation.

This method is very effective in removing the effects of convection as long as flow is laminar and velocity fluctuations during the experiment time are negligible. It has two distinct disadvantages though. First, since the convection compensated scheme requires two subsequent STEs to be applied, each inherently reducing the signal by a factor of two, the total inherent signal reduction will be a factor of four compared to a spin-echo experiment when relaxation is not taken into account. This can significantly increase the required measurement time to achieve an adequate signal-to-noise ratio throughout the attenuation profile. Second, the many rf-pulses required necessitate an extensive phase cycle (50), making the experiment inherently long even when the signal-to-noise ratio does not require that many scans. In addition, when it is electrophoretic migration that needs to be measured in the presence of convection, this pulse sequence is apparently useless, as the effects of the former transport process will be cancelled out as well. However, the simple solution here would be to reverse the polarity of the electrostatic field between the two STE sequences (61).

A convection compensated sequence using bipolar gradients has also been described (60), with two subsequent bipolar gradient STEs [Fig. 7(b)]. Note that the end of the first and the beginning of the second STE are combined into a single spin-echo segment as to reduce the number of rf-pulses. This implies that the two bipolar gradient pulses in this middle segment now each consist of two single gradient pulses with the same polarity, but opposite in sign relative to one another. The intergradient delay within these inner bipolar gradient pulses τ_2 and the delay within the outer bipolar gradient pulses τ_1 are often slightly different due to the absence of the 180° pulse in τ_2. Similarly as for the monopolar gradient sequence, the diffusion attenuation equation is then the product of the attenuation equations of each individual bipolar gradient STE sequence, taking a diffusion delay of $\Delta/2$ per STE and the different τ values into account

$$E_{\text{diff}} = e^{-D\gamma^2\delta^2\sigma^2 g^2\left[\Delta+\frac{2\kappa-2\lambda-\delta}{2}-\frac{\tau_1+\tau_2}{2}\right]}. \quad [65]$$

Other convection compensated pulse sequences have been introduced as well (*vide infra*). Instead of a double STE sequence, a double spin-echo sequence can be used as well to compensate for convection, which does not have the disadvantage of inherently losing a factor of four in signal. CONVEX (62) is one example of such a double spin echo, which simultaneously provides for solvent suppression through excitation sculpting.

Overview

In Table 2, the ST equations with the generalized gradient shape parameters derived for all previous cases are summarized. The variable parts of these equations, $\sigma^2 \times \Delta'$, are explicitly calculated for all gradient shapes listed in Table 1. Table 2 can therefore be regarded as a useful quick reference chart.

MODIFIED DIFFUSION NMR EXPERIMENTS

Many pulse sequences have been proposed over the years that further improve upon the diffusion NMR experiment. Often, their gradient pattern is similar to those of the pulse sequences discussed above so that the ST equation remains unaffected. Examples include: modifications to remove the lineshape distortion effects of homonuclear scalar coupling evolution during the pulse sequence (63–65); removal of the multiplet structure by homonuclear decoupling, strongly increasing the chemical shift resolution of the spectra (66); or 3D DOSY spectra, where the diffusion NMR experiment is combined with a classical 2D NMR type experiment (35–37, 67–77). Table 3 provides an overview of most of these experiments, and points out which ST equation should be applied.

On the other hand, when designing new experiments, it is often necessary to include additional gradient pulses for the purpose of CTP or signal selection. When the coherence order of the selected CTP is nonzero during these pulses, they may interfere with the $q(t)$ function and thus with the resulting ST equation. If they are applied in such a way that they do not influence the $q(t)$ function between the start of the diffusion encoding gradient pulse and the end of the diffusion decoding gradient pulse, then they will just add a constant term to the ST equation. These can be safely ignored for the purpose of determining diffusion coefficients through variation of the encoding/decoding gradient strength, as the extra diffusion attenuation is constant can be absorbed entirely in the pre-exponential term of the signal intensity

Table 2 Overview of $\sigma^2 \times \Delta'$ for the Most Common Diffusion Pulse Sequences as a Function of Gradient Shape

Gradient pattern	Monopolar	Bipolar	Unbalanced bipolar (one-shot)[a]	Double Monopolar	Double Bipolar[b]
Generalized gradient shape parameters	$\sigma^2[\Delta + 2(\kappa - \lambda)\delta]$	$\sigma^2\left[\Delta + \frac{(2\kappa-2\lambda-1)\delta}{4} - \frac{\tau}{2}\right]$	$\sigma^2\left[\Delta + \frac{(\kappa-\lambda)(\alpha^2(1+m^2)+2)\delta}{4} + \frac{(\delta+2\tau)}{8}\left(\alpha^2(1+m^2) + 2\alpha(1-m) - 2\right)\right]$	$\sigma^2[\Delta + 4(\kappa - \lambda)\delta]$	$\sigma^2\Delta + \frac{(2\kappa-2\lambda-1)\delta}{2} - \frac{\tau_1+\tau_2}{2}$
Rectangle	$\left[\Delta - \frac{\delta}{3}\right]$	$\left[\Delta - \frac{\delta}{3} - \frac{\tau}{2}\right]$	$\left[\Delta - \frac{(2-\alpha^2)\delta}{6} - \frac{\tau(1-\alpha^2)}{2}\right]$	$\left[\Delta - \frac{2\delta}{3}\right]$	$\left[\Delta - \frac{2\delta}{3} - \frac{\tau_1+\tau_2}{2}\right]$
Sine bell	$\frac{4}{\pi^2}\left[\Delta - \frac{\delta}{4}\right]$	$\frac{4}{\pi^2}\left[\Delta - \frac{5\delta}{16} - \frac{\tau}{2}\right]$	$\frac{4}{\pi^2}\left[\Delta - \frac{(5-3\alpha^2)\delta}{16} - \frac{\tau(1-\alpha^2)}{2}\right]$	$\frac{4}{\pi^2}\left[\Delta - \frac{\delta}{2}\right]$	$\frac{4}{\pi^2}\left[\Delta - \frac{5\delta}{8} - \frac{\tau_1+\tau_2}{2}\right]$
Square sine bell	$\frac{1}{4}\left[\Delta - \left(\frac{1}{3} - \frac{5}{4\pi^2}\right)\delta\right]$	$\frac{1}{4}\left[\Delta - \left(\frac{1}{3} - \frac{5}{16\pi^2}\right)\delta - \frac{\tau}{2}\right]$	$\frac{1}{4}\left[\Delta - \frac{\left(\left(2-\frac{15}{8\pi^2}\right) - \left(1+\frac{15}{8\pi^2}\right)\alpha^2\right)\delta}{6} - \frac{\tau(1-\alpha)}{2}\right]$	$\frac{1}{4}\left[\Delta - \left(\frac{2}{3} - \frac{5}{2\pi^2}\right)\delta\right]$	$\frac{1}{4}\left[\Delta - \left(\frac{2}{3} - \frac{5}{8\pi^2}\right)\delta - \frac{\tau_1+\tau_2}{2}\right]$
Trapezoid	$\frac{81}{100}\left[\Delta - \frac{3,667\delta}{12,150}\right]$	$\frac{81}{100}\left[\Delta - \frac{15,817\delta}{48,600} - \frac{\tau}{2}\right]$	$\frac{81}{100}\left[\Delta - \frac{(15,817-8,483\alpha^2)\delta}{48,600} - \frac{\tau(1-\alpha^2)}{2}\right]$	$\frac{81}{100}\left[\Delta - \frac{3,667\delta}{6,075}\right]$	$\frac{81}{100}\left[\Delta - \frac{15,817\delta}{24,300} - \frac{\tau_1+\tau_2}{2}\right]$
Smoothed rectangle	$\frac{81}{100}\left[\Delta - \frac{1,484\pi^2-207}{4,860\pi^2}\delta\right]$	$\frac{81}{100}\left[\Delta - \frac{6,344\pi^2-207}{19,440\pi^2}\delta - \frac{\tau}{2}\right]$	$\frac{81}{100}\left[\Delta - \frac{[(3,367\pi^2-207)\alpha^2+(6,344\pi^2-207)\delta]}{19,440\pi^2} - \frac{\tau(1-\alpha^2)}{2}\right]$	$\frac{81}{100}\left[\Delta - \frac{1,484\pi^2-207}{2,430\pi^2}\delta\right]$	$\frac{81}{100}\left[\Delta - \frac{6,344\pi^2-207}{9,720\pi^2}\delta - \frac{\tau_1+\tau_2}{2}\right]$

[a] For calculation, it is assumed that $m = +1$.

[b] Assuming two consecutive bipolar SE or STE sequences with equal diffusion delays $\Delta/2$.

Table 3   Overview of Published Diffusion NMR Experiments with Appropriate ST Equation

Purpose	Reference	Gradient pattern	ST equation[a]
Reduction of eddy currents by LED sequence			
LED	(78)	Monopolar	
BBP-LED	(79)	Bipolar	
Double STE LED	(60)	Double monopolar or bipolar	$-D\gamma^2\delta^2\sigma g_1^2[\Delta_1(1+C)+2(\kappa-\lambda)(1+C)^2\delta]$
Solvent suppression			
Excitation sculpting	(80)	Bipolar	
Excitation sculpting & convection compensation (CONVEX)	(40, 62)	Double monopolar[b]	$-D\gamma^2\delta^2\sigma^2\left[\Delta(g_1-g_2)^2+2\delta(\kappa-\lambda)(g_1^2+g_2^2)\right.$
PGSTE-WATERGATE	(81)	Unbalanced bipolar[b,c]	$\left.+(\delta+2\delta_2)(g_1^2-g_2^2+2g_1g_2)\right]$
Double echo PGSTE-WATERGATE	(59)	Double Unbalanced bipolar[b,c]	$-D\gamma^2\delta^2\sigma^2\left[\Delta(g_1-g_2)^2+4\delta(\kappa-\lambda)(g_1^2+g_2^2)\right.$ $\left.+2(\delta+2\delta_2)(g_1^2-g_2^2+2g_1g_2)\right]$
Heteronuclear 1D			
DEPT-spin echo	(82)	Monopolar	
INEPT-IDOSY	(75)	Quadruple monopolar[b]	$-D\gamma^2\delta^2\sigma^2 g_1^2[\Delta+8(\kappa-\lambda)\delta]$
Multi-quantum-PGSTE	(83)	bipolar[b,d]	$-D(\gamma_{13C}+n\gamma_{1H})^2\delta^2\sigma^2 g^2[4\Delta+4(\kappa-\lambda)\delta-2\tau']$
Removal of *J*-coupling evolution artifacts			
Based on spin-lock, homospoil gradient or chirp z-filter	(64, 65)	Monopolar	
One-shot45	(63)	Unbalanced bipolar	
Increasing chemical shift resolution			
Pure chemical shift DOSY	(66)	Monopolar	
Selective TOCSY-DOSY	(68)	Bipolar	
Saturation Transfer Difference (STD) DOSY	(84)	Bipolar	
Double quantum filter	(40, 85)	Other[b]	$-D\gamma^2\delta^2\sigma^2 g^2[PU+QT+Vx+Wy-3(\kappa-\lambda)R\delta]$

(Continued)

Table 3 (*Continued*)

Purpose	Reference	Gradient pattern	ST equation[a]
3D DOSY experiments			
2D J-resolved DOSY	(70)	Bipolar	
2D J-resolved IDOSY	(73)	Monopolar	
Convection compensated 2D J-resolved IDOSY	(74)	Quadruple monopolar[b]	$-D\gamma^2\delta^2\sigma^2 g\ [\Delta_1 + \Delta_2 + 8\ (\kappa - \lambda)\delta]$
COSY-DOSY	(77)	Bipolar	
COSY-IDOSY	(72)	Monopolar	$-D\gamma^2\delta^2\sigma^2 g^2\ [\Delta_1 + \Delta_2 + 8\ (\kappa - \lambda)\delta]$
Convection compensated COSY-IDOSY	(74)	Quadruple monopolar[b]	
DQF-COSY-IDOSY	(71)	Monopolar or other[e]	$-D\gamma^2\{\delta^2 g^2\sigma^2[\Delta + 2(\kappa - \lambda)\delta]$ $+ \delta_{CTP}^2 g_{CTP}^2\sigma_{CTP}^2[(2\kappa_{CTP} - 2\lambda_{CTP} + 1)\delta_{CTP} + \tau_2]$ $+ 2\delta\sigma\delta_{CTP}g_{CTP}\sigma_{CTP}[\delta_{CTP} + \tau_2]\}$
DOSY-NOESY	(69)	Monopolar	
TOCSY-DOSY	(68)	Bipolar	
TOCSY-DOSY	(76)	Monopolar	
HMQC-DOSY	(67)	Monopolar	
HMQC-IDOSY	(75)	Quadruple monopolar[b]	$-D\gamma^2\delta^2\sigma^2 g\ [\Delta + 8(\kappa - \lambda)\delta]$
CT-HSQC-IDOSY	(37)	Other[f]	$-D\gamma_H^2\left\{\delta^2 g^2\sigma^2\left[\Delta + \dfrac{(2\kappa - 2\lambda - 1)\delta}{4} - \dfrac{\tau'}{2}\right]\right.$ $+ \delta_{CTP}^2 g_{CTP2}^2\sigma_{CTP}^2[(2\kappa_{CTP} - 2\lambda_{CTP} + 1)\delta_{CTP} + \delta + \tau' + x + y]$ $\left. -\delta g\sigma\delta_{CTP}g_{CTP2}\sigma_{CTP}\left[\dfrac{3}{2} - \lambda\delta + 2x + \tau' + (2\lambda_{CTP}\delta_{CTP})\right]\right\}$

(*Continued*)

Table 3 (Continued)

Purpose	Reference	Gradient pattern	ST equation[a]
CT-HSQC-IDOSY	(35)	Other[b]	$-D\gamma^2\delta^2\sigma^2\left[g^2\left[\Delta+\dfrac{2(\kappa-\lambda)(1+\alpha^2)\delta}{4}+\dfrac{(\delta+2\tau)(\alpha^2-2\alpha-1)}{4}\right]\right.$ $+g_3^2\left[\dfrac{(\kappa-2\lambda+1)\delta}{8}+\dfrac{\kappa\delta_2+\tau_2}{4}\right]$ $\left.\left.-gg_3\left[\dfrac{((1+\alpha)\kappa-(3+\alpha)\lambda+2)\delta}{4}+\delta_2\lambda+\tau_2\right]\right]\right]$
DOSY-TROSY	(36)	Bipolar	

[a] Only explicitly provided when the gradient pattern deviates from those discussed in this paper.

[b] All parameters (including Δ, δ, and τ) are defined as in the original reference, except κ and λ, which are always as defined in Table 1.

[c] This sequence relates to the unbalanced bipolar sequence as discussed in this article, with $m=-1$, $\alpha=(g_1+g_2)/(g_1-g_2)$, $g=(g_2-g_1)/2$, $\tau=2\delta_2$ and δ in the original reference corresponding to $\delta/2$ in this paper.

[d] The parameter n corresponds to the number of attached ^{1}H's to the ^{13}C nucleus.

[e] When the gradient pulses for CTP selection are applied in a direction orthogonal to the gradient pulses for diffusion encoding/decoding, then the ST equation for the monopolar gradient pattern applies. When all gradient pulses are applied in the same direction, the ST equation is as displayed here, with g_{CTP} and δ_{CTP} the strength and duration of the CTP selection gradient pulses, σ_{CTP}, κ_{CTP}, and λ_{CTP} its gradient shape factor and parameters, and τ_2 the delay between the end of the first CTP selection gradient pulse and the start of the second one.

[f] Here, it is assumed that the strength of the first selection gradient pulse g_{CTP1} and second one g_{CTP2} are related as $g_{CTP1}/g_{CTP2}=\gamma_H/\gamma_C$. δ_{CTP} is defined as the duration of these gradient pulses, σ_{CTP}, κ_{CTP}, and λ_{CTP} its gradient shape factor and parameters, τ' is the delay between the two gradient pulses within the bipolar gradient pulse for diffusion encoding/decoding, x is the delay between the end of the first CTP selection gradient pulse and the start of the second diffusion encoding/decoding bipolar gradient pulse, and y is the delay between the end of the second diffusion encoding/decoding bipolar gradient pulse and the start of the final CTP selection gradient pulse.

decay. This condition is not fulfilled when the CTP selection through the additional gradient pulses occurs across or during the encoding/decoding segment. In such cases, inseparable cross-terms between the diffusion attenuation by the encoding/decoding gradients and the additional CTP selection gradients may be introduced in the ST equation, leading to a decay that no longer has its minimum attenuation at $g = 0$. An example is the constant-time-HSQC-IDOSY sequence (37), where the echo–antiecho gradient pulse is located within the diffusion delay, effectively requiring the reevaluation of the ST equation as pointed out later by other authors (35). One way to avoid all of this is to apply the additional gradient pulses in a direction orthogonal to that of the encoding/decoding gradient pulses, e.g., gradients along the x-axis instead of the usual z-axis, so that they will not sample diffusion in the same direction and cannot interfere. This is suggested for the 3D DQF-COSY-IDOSY experiment (71) for instance. Standard NMR probe heads are typically not designed to generate gradient pulses in the x- or y-direction, so usually applying a modified ST equation is the most straightforward solution. Table 3 includes the solution for the ST equations with the generalized gradient shape parameters for those experiments that require a modified version.

In a similar way as CTP selection gradient pulses, constant background magnetic field gradients in the sample can also interfere with the $q(t)$ function, creating both additional and cross-terms in the ST equation (52). Background gradients may originate from magnetic susceptibility heterogeneities in the sample or simply from poor shimming. They also have the property of altering the $q(t)$ function between experiments possessing different CTPs, even though the effective gradient pulse pattern and thus the effective ST equation in the absence of background gradients is the same. Different diffusion attenuations will be detected for instance between spin echo and STE experiments. Experiments where the CTP spends a longer time as nonzero coherence order will be more affected by background gradients. Also, the ST equation of pulse sequences based on bipolar gradient pulses turn out to be the least affected by cross-terms, or not at all when the gradients are placed symmetrically around the $180°$ pulses (86), illustrating yet another advantage of this type of gradient pulse. The review by Zheng and Price (86) provides an overview of the impact of background gradients on diffusion measurements and of the multiple pulse sequences attempting to minimize these effects.

Finally, it should be noted that other pulse sequences exist that measure diffusion based on the same principles as outlined in this article, but in such a different way that the ST equation does not directly come into play. Loening et al. have designed an experiment that encodes the diffusion coefficient in the resonance line shape instead of a signal intensity attenuation (87). Another example is the single-scan DOSY experiment (88), where the signal attenuation itself is obtained through spatial encoding.

CONCLUSION

Diffusion NMR and 2D DOSY experiments have become more and more widely applied over the years, having found its way to the NMR toolbox applied by researchers in different fields of chemistry (polymer chemistry, physical chemists, biomolecular chemistry, etc.). Since the basic spin-echo experiment designed by Stejskal and Tanner and the presentation of the now famous equation bearing their names almost half a century ago, numerous modifications and extensions have been developed to further improve the quality and applicability of this technique. Each such modification requires a critical reassessment of the ST equation. Despite diffusion measurements by NMR have become so common, this is often overlooked. Moreover, the use of shaped gradient pulses also has an impact on the ST equation. For some major manufacturers of NMR instruments, non-rectangular gradient shapes are the standard setting. The gradient shape factor σ is today typically taken into account in the processing software provided by them, but further modifications that would be required are disregarded. Hopefully, this article will contribute to the awareness of this fact. In addition, the introduction of the generalized gradient shape parameters κ and λ provides an easy way of presenting the ST equation independent on gradient shape. Not only does this allow for users to very quickly derive the appropriate ST equation for their particular choice of gradient shape, it also makes it more straightforward for researchers designing novel diffusion NMR experiments to present the ST equation. No longer do they need to go through the tiresome mathematical derivation for each gradient shape or leave it to the user to do so. Presenting the ST equation in this way will also further increase awareness of the gradient shape dependence.

ACKNOWLEDGMENT

REFERENCES

1. Cohen Y, Avram L, Frish L. 2005. Diffusion NMR spectroscopy in supramolecular and combinatorial chemistry: an old parameter—new insights. Angew Chem Int Ed 44(4):520–554.

2. Li DY, Kagan G, Hopson R, Williard PG. 2009. Formula weight prediction by internal reference diffusion-ordered NMR spectroscopy (DOSY). J Am Chem Soc 131:5627–5634.

3. Li DY, Keresztes I, Hopson R, Williard PG. 2009. Characterization of reactive intermediates by multinuclear diffusion-ordered NMR spectroscopy (DOSY). Acc Chem Res 42:270–280.

4. Pregosin PS. 2006. Ion pairing using PGSE diffusion methods. Prog Nucl Magn Reson Spectrosc 49:261–288.

5. Auge S, Schmit PO, Crutchfield CA, Islam MT, Harris DJ, Durand E, et al. 2009. NMR measure of translational diffusion and fractal dimension. Application to molecular mass measurement. J Phys Chem B 113:1914–1918.

6. Cabrita EJ, Berger S. 2002. HR-DOSY as a new tool for the study of chemical exchange phenomena. Magn Reson Chem 40:S122–S127.

7. Cabrita EJ, Berger S, Brauer P, Karger J. 2002. High-resolution DOSY NMR with spins in different chemical surroundings: influence of particle exchange. J Magn Res 157:124–131.

8. Johnson CS. 1993. Effects of chemical-exchange in diffusion-ordered 2D NMR-spectra. J Magn Res Ser A 102:214–218.

9. Fielding L. 2003. NMR methods for the determination of protein-ligand dissociation constants. Curr Top Med Chem 3:39–53.

10. Lucas LH, Larive CK. 2004. Measuring ligand-protein binding using NMR diffusion experiments. Concept Magn Reson A 20:24–41.

11. Soderman O, Stilbs P, Price WS. 2004. NMR studies of surfactants. Concept Magn Reson Part A 23:121–135.

12. Momot KI, Kuchel PW. 2003. Pulsed field gradient nuclear magnetic resonance as a tool for studying drug delivery systems. Concept Magn Reson Part A 19:51–64.

13. Saveyn P, Cocquyt E, Sinnaeve D, Martins JC, Topgaard D, Van der Meeren P. 2008. NMR study of the sorption behavior of benzyl alcohol derivatives into sonicated and extruded dioctadecyldimethylammonium chloride (DODAC) dispersions: the relevance of membrane fluidity. Langmuir 24:3082–3089.

14. Saveyn P, De Geeter J, Sinnaeve D, Van der Meeren P, Martins JC. 2009. Influence of the vesicular bilayer structure on the sorption of ethylbenzyl alcohol. Langmuir 25:11322–11327.

15. Antalek B. 2006. Accounting for spin relaxation in quantitative pulse gradient spin echo NMR mixture analysis. J Am Chem Soc 128:8402–8403.

16. Ribot F, Escax V, Roiland C, Sanchez C, Martins JC, Biesemans M, et al. 2005. In situ evaluation of interfacial affinity in CeO2-based hybrid nanoparticles by pulsed field gradient NMR. Chem Commun 1019–1021.

17. Khajeh M, Botana A, Bernstein MA, Nilsson M, Morris GA. 2010. Reaction kinetics studied using diffusion-ordered spectroscopy and multiway chemometrics. Anal Chem 82:2102–2108.

18. Nilsson M, Khajeh M, Botana A, Bernstein MA, Morris GA. 2009. Diffusion NMR and trilinear analysis in the study of reaction kinetics. Chem Commun 1252–1254.

19. Chakraborty D, Choudhury RP, Schonhoff M. 2010. Adsorption of aromatic alcohols into the walls of hollow polyelectrolyte capsules. Langmuir 26:12940–12947.

20. Choudhury RP, Schonhoff M. 2007, Pulsed field gradient NMR study of phenol binding and exchange in dispersions of hollow polyelectrolyte capsules. J Chem Phys 127, Artn 234702. DOI: 10.1063/1.2807239.

21. Schonhoff M, Soderman O. 1997. PFG-NMR diffusion as a method to investigate the equilibrium adsorption dynamics of surfactants at the solid/liquid interface. J Phys Chem B 101:8237–8242.

22. Morris KF, Johnson CS. 1992. Diffusion-ordered two-dimensional nuclear-magnetic-resonance spectroscopy. J Am Chem Soc 114:3139–3141.

23. Lin MF, Shapiro MJ. 1996. Mixture analysis in combinatorial chemistry. Application of diffusion-resolved NMR spectroscopy. J Org Chem 61:7617–7619.

24. Johnson CS. 1999. Diffusion ordered nuclear magnetic resonance spectroscopy: principles and applications. Prog Nucl Magn Reson Spectrosc 34:203–256.

25. Gostan T, Moreau C, Juteau A, Guichard E, Delsuc MA. 2004. Measurement of aroma compound self-diffusion in food models by DOSY. Magn Reson Chem 42:496–499.

26. Nilsson M, Duarte IF, Almeida C, Delgadillo I, Goodfellow BJ, Gil AM, et al. 2004. High-resolution NMR and diffusion-ordered spectroscopy of port wine. J Agric Food Chem 52:3736–3743.

27. Jerschow A, Muller N. 1998. Diffusion-separated nuclear magnetic resonance spectroscopy of polymer mixtures. Macromolecules 31:6573–6578.

28. Antalek B. 2002. Using pulsed gradient spin echo NMR for chemical mixture analysis: how to obtain optimum results. Concept Magn Reson 14:225–258.

29. Price WS. 1997. Pulsed-field gradient nuclear magnetic resonance as a tool for studying translational diffusion. I. Basic theory. Concept Magn Reson 9:299–336.

30. Price WS. 1998. Pulsed-field gradient nuclear magnetic resonance as a tool for studying translational diffusion. II. Experimental aspects. Concept Magn Reson 10:197–237.

31. Stilbs P. 1987. Fourier transform pulsed-gradient spin-echo studies of molecular diffusion. Prog Nucl Magn Reson Spectrosc 19:1–45.

32. Price WS. 2009. NMR studies of translational motion. Principles and Applications. In:Saykally R, Zewail A, King D, eds. Cambridge: Cambridge University Press.

33. Stejskal EO, Tanner JE. 1965. Spin diffusion measurements: spin echoes in the presence of a time-dependent field gradient. J Chem Phys 42:288–292.

34. Nilsson M. 2009. The DOSY toolbox: a new tool for processing PFG NMR diffusion data. J Magn Res 200:296–302.

35. McLachlan AS, Richards JJ, Bilia AR, Morris GA. 2009. Constant time gradient HSQC-iDOSY: practical aspects. Magn Reson Chem 47:1081–1085.

36. Didenko T, Boelens R, Rüdiger SGD. 2011. 3D DOSY-TROSY to determine the translational diffusion coefficient of large protein complexes. Protein Eng Des Sel 24:99–103.

37. Vitorge B, Jeannerat D. 2006. NMR diffusion measurements in complex mixtures using constant-time-HSQC-IDOSY and computer-optimized spectral aliasing for high resolution in the carbon dimension. Anal Chem 78:5601–5606.

38. Merrill MR. 1993. NMR diffusion measurements using a composite gradient PGSE sequence. J Magn Res Ser A 103:223–225.

39. Price WS, Kuchel PW. 1991. Effect of nonrectangular field gradient pulses in the Stejskal and Tanner (Diffusion) pulse sequence. J Magn Res 94:133–139.

40. Momot KI, Kuchel PW. 2006. PFG NMR diffusion experiments for complex systems. Concept Magnetic Reson Part A 28:249–269.

41. Keeler J, Clowes RT, Davis AL, Laue ED. 1994. Pulsed-field gradients—theory and practice. Nucl Magn Reson C 239:145–207.

42. Croasmun WR, Carlson RMK, eds. 1994. Two-Dimensional NMR Spectroscopy: Application for Chemists and Biochemists, 2nd ed. Wiley-VCH: New York. 980 p.

43. Hahn EL. 1950. Spin echoes. Phys Rev 80:580–594.

44. Baldwin AJ, Christodoulou J, Barker PD, Dobson CM, Lippens G. 2007 Contribution of rotational diffusion to pulsed field gradient diffusion measurements. J Chem Phys 127, Artn 114505. DOI: 10.1063/1.2759211.

45. Dill KA, Bromberg S. 2003. Molecular driving forces: statistical thermodynamics in chemistry and biology. New York: Garland Science.

46. Morris KF, Johnson CS. 1992. Mobility-ordered two-dimensional nuclear-magnetic-resonance spectroscopy. J Am Chem Soc 114:776–777.

47. Torrey HC. 1956. Bloch equations with diffusion terms. Phys Rev 104:563.

48. Jerschow A. 2000. Thermal convection currents in NMR: flow profiles and implications for coherence pathway selection. J Magn Res 145:125–131.

49. Loening NM, Keeler J. 1999. Measurement of convection and temperature profiles in liquid samples. J Magn Res 139:334–341.

50. Connell MA, Bowyer PJ, Bone PA, Davis AL, Swanson AG, Nilsson M, Morris GA. 2009. Improving the accuracy of pulsed field gradient NMR diffusion experiments: correction for gradient non-uniformity. J Magn Res 198:121–131.

51. Damberg P, Jarvet J, Graslund A. 2001. Accurate measurement of translational diffusion coefficients: a practical method to account for nonlinear gradients. J Magn Res 148:343–348.

52. Price WS, Stilbs P, Jonsson B, Soderman O. 2001. Macroscopic background gradient and radiation damping effects on high-field PGSE NMR diffusion measurements. J Magn Res 150:49–56.

53. Tanner JE. 1970. Use of stimulated echo in NMR-diffusion studies. J Chem Phys 52:2523–2526.

54. Cotts RM, Hoch MJR, Sun T, Markert JT. 1989. Pulsed field gradient stimulated echo methods for improved NMR diffusion measurements in heterogeneous systems. J Magn Res 83:252–266.

55. Karlicek RF, Lowe IJ. 1980. Modified pulsed gradient technique for measuring diffusion in the presence of large background gradients. J Magn Res 37:75–91.

56. Chen AD, Johnson CS, Lin M, Shapiro MJ. 1998. Chemical exchange in diffusion NMR experiments. J Am Chem Soc 120:9094–9095.

57. Sinnaeve D, Hendrickx PMS, Van hemel J, Peys E, Kieffer B, Martins JC. 2009. The solution structure and self-association properties of the cyclic lipodepsipeptide pseudodesmin A support its pore-forming potential. Chem—Eur J 15:12653–12662.

58. Pelta MD, Morris GA, Stchedroff MJ, Hammond SJ. 2002. A one-shot sequence for high-resolution diffusion-ordered spectroscopy. Magn Reson Chem 40:S147–S152.

59. Zheng G, Price WS. 2009. Simultaneous convection compensation and solvent suppression in biomolecular NMR diffusion experiments. J Biomol NMR 45:295–299.

60. Jerschow A, Muller N. 1997. Suppression of convection artifacts in stimulated-echo diffusion experiments. Double-stimulated-echo experiments. J Magn Res 125:372–375.

61. He QH, Wei ZH. 2001. Convection compensated electrophoretic NMR. J Magn Res 150:126–131.

62. Momot KI, Kuchel PW. 2004. Convection-compensating PGSE experiment incorporating excitation-sculpting water suppression (CONVEX). J Magn Res 169:92–101.

63. Botana A, Aguilar JA, Nilsson M, Morris GA. 2011. J-modulation effects in DOSY experiments and their suppression: the Oneshot45 experiment. J Magn Res 208:270–278.

64. Torres AM, Dela Cruz R, Price WS. 2008. Removal of J-coupling peak distortion in PGSE experiments. J Magn Res 193:311–316.

65. Torres AM, Zheng G, Price WS. 2010. J-compensated PGSE: an improved NMR diffusion experiment with fewer phase distortions. Magn Reson Chem 48:129–133.

66. Nilsson M, Morris GA. 2007. Pure shift proton DOSY: diffusion-ordered ^{1}H spectra without multiplet structure. Chem Commun 933–935.

67. Barjat H, Morris GA, Morris GA. 1998. A three-dimensional DOSY-HMQC experiment for the high-resolution analysis of complex mixtures. J Magn Res 131:131–138.

68. Bradley SA, Krishnamurthy K, Hu H. 2005. Simplifying DOSY spectra with selective TOCSY edited preparation. J Magn Res 172:110–117.

69. Gozansky EK, Gorenstein DG. 1996. DOSY-NOESY: diffusion-ordered NOESY. J Magn Res Ser B 111:94–96.

70. Lucas LH, Otto WH, Larive CK. 2002. The 2D-J-DOSY experiment: resolving diffusion coefficients in mixtures. J Magn Res 156:138–145.

71. Newman JM, Jerschow A. 2007. Improvements in complex mixture analysis by NMR: DQF-COSY iDOSY. Anal Chem 79:2957–2960.

72. Nilsson M, Gil AM, Delagadillo I, Morris GA. 2005. Improving pulse sequences for 3D DOSY: COSY-IDOSY. Chem Commun 1737–1739.

73. Nilsson M, Gil AM, Delgadillo I, Morris GA. 2004. Improving pulse sequences for 3D diffusion-ordered NMR spectroscopy: 2DJ-IDOSY. Anal Chem 76:5418–5422.

74. Nilsson M, Morris GA. 2005. Improving pulse sequences for 3D DOSY: convection compensation. J Magn Res 177:203–211.

75. Stchedroff MJ, Kenwright AM, Morris GA, Nilsson M, Harris RK. 2004. 2D and 3D DOSY methods for studying mixtures of oligomeric dimethylsiloxanes. Phys Chem Chem Phys 6:3221–3227.

76. Viel S, Caldarelli S. 2008. Improved 3D DOSY-TOCSY experiment for mixture analysis. Chem Commun 2013–2015.

77. Wu DH, Chen AD, Johnson CS. 1996. Three-dimensional diffusion-ordered NMR spectroscopy: the homonuclear COSY-DOSY experiment. J Magn Res Ser A 121:88–91.

78. Gibbs SJ, Johnson CS. 1991. A PFG NMR experiment for accurate diffusion and flow studies in the presence of eddy currents. J Magn Res 93:395–402.

79. Wu DH, Chen AD, Johnson CS. 1995. An improved diffusion-ordered spectroscopy experiment incorporating bipolar-gradient pulses. J Magn Res Ser A 115:260–264.

80. Balayssac S, Delsuc MA, Gilard V, Prigent Y, Malet-Martino M. 2009. Two-dimensional DOSY experiment with excitation sculpting water suppression for the analysis of natural and biological media. J Magn Res 196:78–83.

81. Zheng G, Stait-Gardner T, Kumar PGA, Torres AM, Price WS. 2008. PGSTE-WATERGATE: an STE-based PGSE NMR sequence with excellent solvent suppression. J Magn Res 191:159–163.

82. Botana A, Howe PWA, Caer V, Morris GA, Nilsson M. 2011. High resolution ^{13}C DOSY: the DEPTSE experiment. J Magn Res 211:25–29.

83. Zheng G, Torres AM, Price WS. 2009. MQ-PGSTE: a new multi-quantum STE-based PGSE NMR sequence. J Magn Res 198:271–274.

84. Kramer M, Kleinpeter E. 2010. STD-DOSY: a new NMR method to analyze multi-component enzyme/substrate systems. J Magn Res 202:245–249.

85. Momot KI, Kuchel PW. 2005. Convection-compensating diffusion experiments with phase-sensitive double-quantum filtering. J Magn Res 174:229–236.

86. Zheng G, Price WS. 2007. Suppression of background gradients in (B0 gradient-based) NMR diffusion experiments. Concept Magn Reson Part A 30:261–277.

87. Loening NM, Keeler J, Morris GA. 2001. One-dimensional DOSY. J Magn Res 153:103–112.

88. Shrot Y, Frydman L. 2008. Single-scan 2D DOSY NMR spectroscopy. J Magn Res 195:226–231.

BIOGRAPHY

Davy Sinnaeve is a post-doctoral researcher at Ghent University in the NMR and Structure Analysis research group headed by Prof. José C. Martins in the Department of Organic Chemistry. He obtained a Master's degree in 2005 and his PhD in 2010, both in Chemistry. During his PhD, he applied both diffusion and heteronuclear relaxation measurements to study the ordered self-assembly of a cyclic lipodepsi-peptide. His current research interest involves the investigation of the structure–function relationship of this class of compounds and the development of new applications of NMR techniques to study molecular self-assembly in general.